Chapter 6
Redox Transformations and Transport Processes

The elucidation of the nature of charge transfer and charge transport processes in electrochemically active polymer films may be the most interesting theoretical problem of this field. It is also a question of great practical importance, because in most of their applications fast charge propagation through the film is needed. It has become clear that the elucidation of their electrochemical behavior is a very difficult task, due to the complex nature of these systems [1–8].

In the case of traditional electrodes, the electrode reaction involves mass transport of the electroactive species from the bulk solution to the electrode surface and an electron transfer step at the electrode surface. A polymer film electrode can be defined as an electrochemical system in which at least three phases are contacted successively in such a way that between a first-order conductor (usually a metal) and a second-order conductor (usually an electrolyte solution) is an electrochemically active polymer layer. The polymer layer is more or less stably attached to the metal, mainly by adsorption (adhesion).

The fundamental observation that should be explained is that even rather thick polymer films, in which most of the redox sites are as far from the metal surface as 100–10,000 nm (this corresponds to surface concentrations of the redox sites $\Gamma = 10^{-8}$–10^{-6} mol cm^{-2}), may be electrochemically oxidized or reduced.

According to the classical theory of simple electron transfer reactions, the reactants get very close to the electrode surface, and then electrons can tunnel over the short distance (tenths of a nanometer) between the metal and the activated species in the solution phase.

In the case of polymer-modified electrodes, the active parts of the polymer cannot approach the metal surface because polymer chains are trapped in a tangled network, and chain diffusion is usually much slower than the time scale of the transient electrochemical experiment (e.g., cyclic voltammetry). Although we should not exclude the possibility that polymer diffusion may play a role in carrying charges, even the redox sites may get close enough to the metal surface when the film is held together by physical forces. It may also be assumed that in ion exchange polymeric systems, where the redox-active ions are held by electrostatic binding [e.g., $Ru(bpy)_3^{3+/2+}$ in Nafion], some of these ions can reach the metal surface.

G. Inzelt, *Conducting Polymers*, Monographs in Electrochemistry,
DOI 10.1007/978-3-642-27621-7_6,

However, when the redox sites are covalently bound to the polymer chain (i.e., no free diffusion of the sites occurs), and especially when the polymer chains are connected by chemical cross-linkages (i.e., only segmental motions are possible), an explanation of how the electrons traverse the film should be provided.

Therefore, the transport of electrons can be assumed to occur either via an electron exchange reaction (electron hopping) between neighboring redox sites, if the segmental motions make it possible, or via the movement of delocalized electrons through the conjugated systems (electronic conduction). The former mechanism is characteristic of redox polymers that contain covalently attached redox sites, either built into the chain or included as pendant groups, or redox-active ions held by electrostatic binding.

Polymers that possess electronic conduction are called conducting polymers, electronically conducting polymers, or intrinsically conducting polymers—ICPs (see Chap. 2). Electrochemical transformation—usually oxidation—of the nonconducting forms of these polymers usually leads to a reorganization of the bonds of the macromolecule and the development of an extensively conjugated system. An electron hopping mechanism is likely to be operative between the chains (interchain conduction) and defects, even in the case of conducting polymers.

However, it is important to pay attention to more than just the "electronic charging" of the polymer film (i.e., to electron exchange at the metal–polymer interface and electron transport through the surface layer), since ions will cross the film–solution interface in order to preserve electroneutrality within the film. The movement of counterions (or less frequently that of co-ions) may also be the rate-determining step.

At this point, it is worth noting that "electronic charging (or simply charging) the polymer" is a frequently used expression in the literature of conducting polymers. It means that either the polymer backbone or the localized redox sites attached to the polymeric chains will have positive or negative charges as a consequence of a redox reaction (electrochemical or chemical oxidation or reduction) or less often protonation (e.g., "proton doping" in the case of polyaniline). This excess charge is compensated for by the counterions; i.e., the polymer phase is always electrically neutral. A small imbalance of the charge related to the electrochemical double layers may exist only at the interfacial regions. "Discharging the polymer" refers to the opposite process where the electrochemical or chemical reduction or oxidation (or deprotonation) results in an uncharged (neutral) polymer, and, because the counterions leave the polymer film, in a neutral polymer phase.

The thermodynamic equilibrium between the polymer phase and the contacting solutions requires $\tilde{\mu}_i(\text{film}) = \tilde{\mu}_i$ (solution) for all mobile species, as discussed in Chap. 5. In fact, we may regard the film as a membrane or a swollen polyelectrolyte gel (i.e., the charged film contains solvent molecules and, depending on the conditions, co-ions in addition to the counterions).

A simple model of the charge transfer and transport processes in a polymer film electrode is shown in Fig. 6.1.

As a consequence of the incorporation of ions and solvent molecules into the film, swelling or shrinkage of the polymer matrix takes place. Depending on the

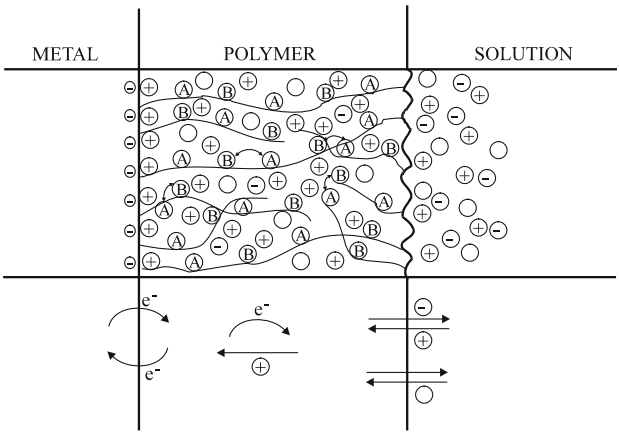

Fig. 6.1 A schematic picture of a polymer film electrode. In an electrochemical experiment, the electron transfer occurs at the metal–polymer interface that initiates the electron propagation through the film via an electron exchange reaction between redox couples A and B or electronic conduction through the polymer backbone. (When the polymer reacts with an oxidant or reductant added to the solution, the electron transfer starts at the polymer–solution interface.) Ion exchange processes take place at the polymer–solution interface; in the simplest case counterions enter the film and compensate for the excess charge of the polymer. Neutral (solvent) molecules (O) may also be incorporated into the film (resulting in swelling) or may leave the polymer layer

nature and the number of cross-links, reversible elastic deformation or irreversible changes (e.g., dissolution) may occur. Other effects, such as dimerization, ion-pair formation, and cross-linking, should also be considered.

We have already mentioned several effects that are connected with the polymeric nature of the layer. It is evident that all the charge transport processes listed are affected by the physicochemical properties of the polymer. Therefore, we also must deal with the properties of the polymer layer if we wish to understand the electrochemical behavior of these systems. The elucidation of the structure and properties of polymer (polyelectrolyte) layers as well as the changes in their morphology caused by the potential and potential-induced processes and other parameters (e.g., temperature, electrolyte composition) set an entirely new task for electrochemists. Owing to the long relaxation times that are characteristic of polymeric systems, the equilibrium or steady-state situation is often not reached within the time allowed for the experiment.

However, the application of combined electrochemical and nonelectrochemical techniques has allowed very detailed insights into the nature of ionic and electronic charge transfer and charge transport processes.

In this chapter, we intend to outline some relevant experiences, to discuss existing models and theories, and to summarize and systematize the knowledge accumulated on charge transport processes occurring in redox and conducting polymer films.

6.1 Electron Transport

As has already been mentioned, electron transport occurs in redox polymers—which are localized state conductors—via a process of sequential electron self-exchange between neighboring redox groups. In the case of electronically conducting polymers—where the polymer backbone is extensively conjugated, making considerable charge delocalization possible—the transport of the charge carriers along a conjugated strand can be described by the band model characteristic of metals and semiconductors. Besides this intrachain conduction, which provides very high intrinsic conductivity, various hopping and tunneling processes are considered for nonintrinsic (interstrand and interfiber) conduction processes.

6.1.1 Electron Exchange Reaction

The elementary process is the transfer of an electron from an electron donor orbital on the reductant (e.g., Fe^{2+}) to the acceptor orbital of the oxidant (e.g., Fe^{3+}). The rate of electron transfer is very high, taking place within 10^{-16} s; however, bond reorganization may require from 10^{-13} to 10^{-14} s, reorientation of the solvent dipoles (e.g., water molecules in the hydration sphere) needs 10^{-11} to 10^{-12} s, and the duration of the rearrangement of the ionic atmosphere is ca. 10^{-8} s. The rate coefficients are much higher for electron exchange reactions occurring practically without structural changes (outer sphere reactions) than for reactions that require high energies of activation due to bond reorganization (inner sphere mechanism).

However, the probability of electron transfer (tunneling) depends critically on the distance between the species participating in the electron exchange reaction. A reaction can take place between two molecules when they meet each other. It follows that the rate-determining step can be either the mass transport (mostly diffusion is considered, but effect of migration cannot be excluded) or the reaction (the actual rate of electron transfer in our case). For an electron exchange process coupled to isothermal diffusion, the following kinetic scheme may be considered:

$$A + B^- \underset{\overleftarrow{k}_d}{\overset{\vec{k}_d}{\rightleftarrows}} \{AB^-\} \underset{}{\overset{k_e}{\rightleftarrows}} A^- + B, \tag{6.1}$$

where $\vec{k}_d$, $\overleftarrow{k}_d$, and k_e are the rate coefficients for diffusive approach, for separation, and for the forward reaction, respectively. Note that $\vec{k}_d$ is a second-order rate coefficient, while $\vec{k}_d$ and k_e are first-order rate coefficients. The overall second-order rate coefficient can be given by

$$k = \frac{\vec{k}_d k_e}{\overleftarrow{k}_d} + k_e. \tag{6.2}$$

Figure 6.2 schematically illustrates the microscopic events that occur during an electron exchange reaction.

If the reaction has a small energy of activation, so k_e is high ($k_e \gg \overleftarrow{k}_d$), the rate-determining step is the approach of the reactants. Under these conditions, it holds that $k = \vec{k}_d$. The kinetics are activation controlled for reactions with large activation energies ($\Delta G^{\ddagger} > 20$ kJ mol^{-1} for reactions in aqueous solutions), and then

$$k = \frac{k_e \vec{k}_d}{\overleftarrow{k}_d}. \tag{6.3}$$

Since $\vec{k}_d/\overleftarrow{k}_d$ is the equilibrium constant, K for the formation of the precursor complex k can be expressed as

$$k = k_e K. \tag{6.4}$$

The rate of the collision, k_d, can be estimated using Smoluchowski's equation:

$$k_d = 1,000 \times 4\pi N_A r_{AB} D_{AB}, \tag{6.5}$$

where N_A is the Avogadro constant, δ is the mean distance between the centers of the species involved in the electron exchange ($\delta \approx 2r_A$ for identical species where r_A is the radius of the reactant molecule), and D_{AB} is the relative diffusion coefficient of the reacting molecules. The diffusion coefficients of ions in aqueous solutions at 298 K are typically 1–2 $\times$ 10^{-9} m^2 s^{-1}, except $D_{H^+} = 9.1 \times 10^{-9}$ m^2 s^{-1} and $D_{OH^-} = 5.2 \times 10^{-9}$ m^2 s^{-1}. For a small ion $\delta = 0.5$ nm. By inserting these values into (6.5), we obtain $k_d = 8 \times 10^9$ dm^3 mol^{-1} s^{-1}. Consequently,

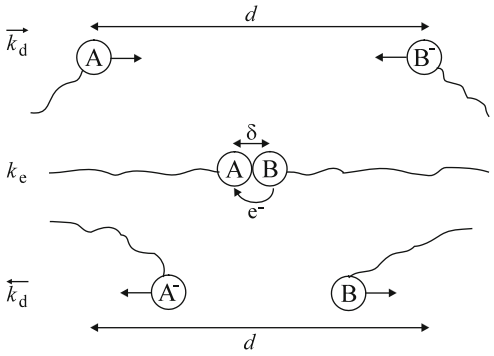

Fig. 6.2 A microscopic-level schematic of the electron exchange process coupled to isothermal diffusion. The *upper part* shows that species A and B$^-$ start to diffuse toward each other from their average equilibrium distance (d) with diffusion rate coefficient, k_d. The next stage is the "forward" electron transfer step after the formation of a precursor complex, characterized by rate coefficient k_e, and the mean distance of the redox centers $\delta = r_A + r_B$ or for similar radii $\delta \cong 2r_A$. The *lower part* depicts the separation of the products, A$^-$ and B

if $k_e > 10^9$ dm^3 mol^{-1} s^{-1} the reaction is diffusion controlled. In aqueous solutions, fast electron transfer and acid–base reactions fall within this category. On the other hand, if the viscosity (η) of the solvent is high, due to the inverse relationship between D and η, k_d may be smaller by orders of magnitude. Similarly, the diffusion of macromolecules is also slow, $D = 10^{-10}$–10^{-16} m^2 s^{-1}. In the case of polymer film electrodes where the polymer chains are trapped in a tangled network, rather small values for the diffusion coefficient of the chain and segmental motions can be expected. If the latter motions are frozen-in (e.g., at low temperatures or without the solvent swelling, which has a plasticizing effect on the polymer film), the electron transport may be entirely restricted.

It follows that diffusion control is more frequently operative in polymeric systems than that in ordinary solution reactions, because k_d and k_e are more likely to be comparable due to the low D values [9–16]. If the electron exchange reaction occurs between ionic species (charged polymer sites), the coulombic forces may reduce or enhance both the probability of the ions encountering each other and the rate of electron transfer. For the activation-controlled case, k_e can be obtained as follows [17]:

$$\ln k_e = \ln k_e^o - \frac{z_A z_B e^2}{2 r_A \varepsilon k_B T}, \tag{6.6}$$

where z_A and z_B are the charges of the ions and ε is the dielectric permittivity of the medium. If z_A and z_B have the same sign k_e decreases; in the opposite case k_e increases. The effect can be modified by using a solvent with high or low ε values or by adding a large amount of inert electrolyte to the solution. In the latter case, the effect of ionic strength (I) is approximately given by

$$\ln k = \ln k^o + z_A z_B A \sqrt{I}, \tag{6.7}$$

where A is the constant of the Debye–Hückel equation, and k^o is the rate coefficient in the absence of electrostatic interactions.

The electron exchange reaction (electron hopping) continuously occurs between the molecules of a redox couple in a random way. Macroscopic charge transport takes place, however, only when a concentration or potential gradient exists in the phase for at least one of the components of the redox couple. In this case, the hydrodynamic displacement is shortened for the diffusive species by $\delta \sim 2r_A$, because the electron exchange (electron diffusion) contributes to the flux. The contribution of the electron diffusion to the overall diffusion flux depends on the relative magnitude of k_e and k_d or D_e and D_{AB} (i.e., the diffusion coefficients of the electron and ions, respectively).

According to the Dahms–Ruff theory of electron diffusion [9–12]

$$D = D_{AB} + D_e = D_{AB} + \frac{k_e \delta^2 c}{6}, \tag{6.8}$$

for three-dimensional diffusion where D is the measured diffusion coefficient, c is the concentration of redox centers, and k_e is the bimolecular electron transfer rate coefficient. The factors 1/4 and 1/2 can be used instead of 1/6 for two- and one-dimensional diffusion, respectively.

This approach has been used in order to describe the electron propagation through surface polymer films [2, 6, 18–26]. In these models, it was assumed that transport occurs as a sequence of successive steps between adjacent redox centers of different oxidation states. The electron hopping has been described as a bimolecular process in the direction of the concentration gradient. The kinetics of the electron transfer at the electrode–polymer film interface, which initiates electron transport in the surface layer, is generally considered to be a fast process which is not rate limiting. It was also presumed that the direct electron transfer between the metal substrate and the polymer involves only those redox sites situated in the layer immediately adjacent to the metal surface. As follows from the theory (6.8), the measured charge transport diffusion coefficient should increase linearly with c whenever the contribution from the electron exchange reaction is important, and so the concentration dependence of D may be used to test theories based on the electron exchange reaction mechanism. Despite the fact that considerable efforts have been made to find the predicted linear concentration dependence of D, it has been observed in only a few cases and for a limited concentration range.

There may be several reasons why this model has not fulfilled expectations although the mechanism of electron transport as described might be correct.

6.1.1.1 Problems with the Verification of the Model

The uncertainty in the determination of D by potential step, impedance, or other techniques is substantial due to problems such as the extraction of D from the product $D^{1/2}c$ (this combination appears in all of the methods), the difficulty arising from the in situ thickness estimation, nonuniform thickness [27–29], film inhomogeneity [30–32], incomplete electroactivity [19, 23, 33], and the ohmic drop effect [34]. It may be forecast, for example, that the film thickness increases, and thus c decreases, due to the solvent swelling the film; however, D_{AB} simultaneously increases, making the physical diffusion of ions and segmental motions less hindered. In addition, the solvent swelling changes with the potential, and it is sensitive to the composition of the supporting electrolyte. Because of the interactions between the redox centers or between the redox species and the film functional groups, the morphology of the film will also change with the concentration of the redox groups. We will deal with these problems in Sects. 6.4–6.7. It is reasonable to assume that in many cases $D_{AB} \gg D_e$ (i.e., the electron hopping makes no contribution to the diffusion), or the most hindered process is the counterion diffusion, coupled to electron transport.

6.1.1.2 Advanced Theories Predicting a Nonlinear $D(c)$ Function

According to the theory of *extended electron transfer* elaborated by Feldberg, δ may be larger than $2r_A$, and this theory predicts an exponential dependence on the average site–site distance (d) (i.e., on the site concentration) [26]:

$$k_e = k_0 \exp \frac{-(d-\delta)}{s}, \tag{6.9}$$

where s is a characteristic distance (ca. 10^{-10} m).

An alternative approach proposed by He and Chen to describe the relationship between the diffusion coefficient and redox site concentration is based on the assumption that at a sufficiently high concentration of redox centers several electron hops may become possible because more than two sites are immediately adjacent. This means that the charge donated to a given redox ion via a diffusional encounter may propagate over more than one site in the direction of the concentration gradient. This is the case in systems where the electron exchange rate is high, and therefore the rate of the electron transport is determined by the physical diffusion of redox species incorporated into the ion exchange membrane or those of the chain and segmental motions. This enhances the total electron flux. Formally, this is equivalent to an increase in the electron hopping distance by a certain factor, f, so D can be expressed as follows [35]:

$$D = D_0 + \frac{k_e c (\delta f)^2}{6}. \tag{6.10}$$

Assuming a Poisson distribution of the electroactive species, the enhancement factor can be expressed as a power series of a probability function which is related to the concentration. At low concentrations, the probability of finding more than one molecule in a hemisphere with a radius of the molecular collision distance is nearly zero and $f = 1$. The factor f, and therefore D_e, increases noticeably at higher concentrations.

Another model introduced by Fritsch-Faules and Faulkner suggests that k_e or D_e should first have an exponential rise with increasing c and then flatten at high concentrations. The exponential rise occurs because d becomes smaller as the concentration increases, which promotes intersite electron transfer. As the minimum center-to-center separation is approached, when each redox center has a nearest neighbor that is practically in contact, k_e or D_e asymptotically approaches its theoretical maximum value. A similar result has been obtained by a microscopic model which describes electron (or hole) diffusion in a rigid three-dimensional network. This concept is based on simple probability distribution arguments and on a random walk [36].

6.1.1.3 Transition Between Percolation and Diffusion Behaviors

Blauch and Savéant systematically investigated the interdependence between physical displacement and electron hopping in propagating charge through supramolecular redox systems [37]. It was concluded that when physical motion is either nonexistent or much slower than electron hopping, charge propagation is fundamentally a percolation process, because the microscopic distribution of redox centers plays a critical role in determining the rate of charge transport [37, 38]. Any self-similarity of the molecular clusters between successive electron hops imparts a memory effect, making the exact adjacent-site connectivity between the molecules important. The redox species can move about their equilibrium positions at which they are irreversibly attached to the polymer (in the three-dimensional network, the redox species are either covalently or electrostatically bound); this is referred to as "bounded diffusion." In the opposite extreme (free diffusion), rapid molecular motion thoroughly rearranges the molecular distribution between successive electron hops, thus leading a mean-field behavior. The mean-field approximation presupposes that $k_d > k_e$ and leads to Dahms–Ruff-type behavior for freely diffusing redox centers, but the following corrected equation should be applied [37]:

$$D = D_{AB}(1 - x)f_c + D_e x, \tag{6.11}$$

where x is the fractional loading, which is the ratio of the total number of molecules to the total number of lattice sites. The factor $(1 - x)$ in the first term accounts for the blocking of physical diffusion and f_c is a correlation factor which depends on x. When D_{AB} becomes less than D_e, percolation effects appear. If $D_e \gg D_{AB}$, a characteristic static percolation behavior ($D = 0$ below the percolation threshold and an abrupt onset of conduction at the critical fractional loading) should be observed. The mechanistic aspects of the charge transport can be understood from D versus x plots. When D_{AB} is low, that is in the case of bounded diffusion [26, 38],

$$D = D_e x = \frac{k_e \delta^2 x^2 c}{6}. \tag{6.12}$$

Thus, D varies with x^2 when the rate of physical diffusion is slow.
In the case of free diffusion, the apparent diffusion coefficient becomes

$$D = D_{AB} f(1 - x). \tag{6.13}$$

Accordingly D will decrease with x. This situation originates in the decreased availability of vacant sites (free volume) within the polymer film. When both electron hopping and physical diffusion processes occur at the same rate ($D_{AB} = D_e$), D becomes invariant with x.

6.1.1.4 Potential Dependence of the Diffusion Coefficient

In the simple models, D_e is independent of the potential because the effects of both the counterion activity and interactions of charged sites (electron–electron interactions) are neglected. However, in real systems, the electrochemical potential of counterions is changed as the redox state of the film is varied, the counterion population is limited, and interactions between electrons arise. According to Chidsey and Murray, the potential dependence of the electron diffusion coefficient can be expressed as follows [39]:

$$D_e = k_e\delta^2\{1 + [z_i^{-1}(x_e - z_s)^{-1} + g/k_BT]x_e(1 - x_e)\}, \tag{6.14}$$

where x_e is the fraction of sites occupied by electrons, z_s and z_i are the charges of the sites and the counterions, respectively, and g is the occupied site interaction energy (The g parameter is similar to that of the Frumkin isotherm.) In the case of noninteracting sites ($g = 0$), and in the presence of a large excess of supporting electrolyte ($z_s = \infty$), $D_e = k_e\delta^2$ and this is a diffusion coefficient. In general, D_e does not remain constant as the potential (that is, the film redox composition) is changed. D_e does not vary substantially with potential within the reasonable ranges of g and z_s (e.g., if $g = 4$, D_e will only be double compared to its value at $g = 0$), and a maximum (if $g > 0$) or a minimum (if $g < 0$) will appear at the standard redox potential of the system.

The details of other theoretical models, including electric field effects [13, 14, 40–46], can be found in [3, 7, 18].

6.1.2 Electronic Conductivity

Electronically conducting polymers consist of polyconjugated, polyaromatic, or polyheterocyclic macromolecules, and these differ from redox polymers in that the polymer backbone is itself electronically conducting in its "doped" state. The term "doping," as it is often applied to the charging process of the polymer, is somewhat misleading. In semiconductor physics, doping describes a process where dopant species present in small quantities occupy positions within the lattice of the host material, resulting in a large-scale change in the conductivity of the doped material compared to the undoped one. The "doping" process in conjugated polymers is, however, essentially a charge transfer reaction, resulting in the partial oxidation (or less frequently reduction) of the polymer. Although conjugated polymers may be charged positively or negatively, studies of the charging mechanism have mostly been devoted to the case of p-doping. The electronic conductivity shows a drastic change (up to 10–12 orders of magnitude) from its low value for the initial (uncharged) state of the polymer, corresponding to a semiconductor or even an insulator, to values of 1–1,000 S cm^{-1} (even up to 10^5 S cm^{-1} comparable

to metals) [47–66]. The range of conductivities of conducting polymers in charged and uncharged states in comparison with different materials (insulators, semiconductors, and metallic conductors) is displayed in Fig. 6.3.

In general, the mobility of initial portions of the incorporated electronic charge is rather low. At higher charging levels, the conductivity increases much more rapidly than the charge and then levels out, or even decreases. This onset of conductivity has been interpreted as an insulator–metal transition due to various electron–electron interactions [67]. The temperature dependence of the conductivity in the highly charged state does not correspond in most cases to the metallic type [68]. In agreement with quantum-chemical expectations, electron spin resonance (ESR) measurements have demonstrated the presence of unpaired spins inside the polymer film. However, the spin concentration passes through a maximum at a relatively low charging level, usually before the high conductivity increase, and then vanishes [52, 69–77]. The variation of the ESR signal intensity (in arbitrary units) during a potential cycle and the corresponding cyclic voltammogram are shown in Fig. 6.4.

As observed in ESR measurements, the generation of polarons (see below) at an early stage of oxidation is widely accepted. However, at higher oxidation levels, the decrease in spin density with increasing conductivity is found to be a challenging feature. The following conclusions were drawn based on the correlation between the mobilities and the ESR signal. The variation in mobility as a function of oxidation level (Figs. 6.5 and 6.6) can be explained by the polaron lattice model [78].

The mobilities were calculated from the relation $\mu = \sigma/\rho_{cc}F$, where σ is the conductivity and ρ_{cc} is the density of charge carriers. The charge-carrier density was estimated from the charge measured by coulometry (Q), the density of the polymer (ρ, which was assumed to be 1 g cm^{-3}), the molar mass of the aniline monomer unit (M), and the weight of the polymer film (W): $\rho_{cc} = \rho Q/FW$.

The sharp rise in the mobility suggests the evolution of metallic conduction, and this is attributed to the formation of Pauli spins. The decrease in ESR intensity at

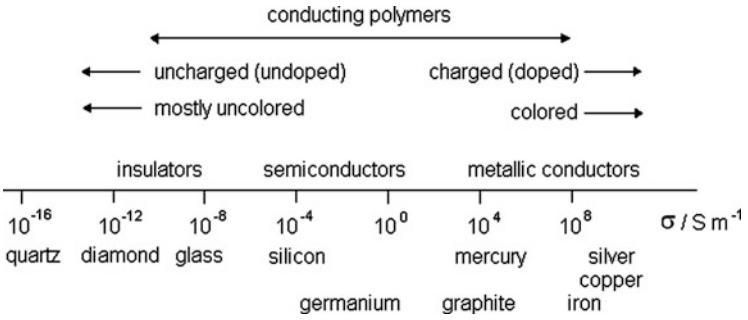

Fig. 6.3 Illustration of the range of electronic conductivities of conducting polymers in comparison with those of other materials

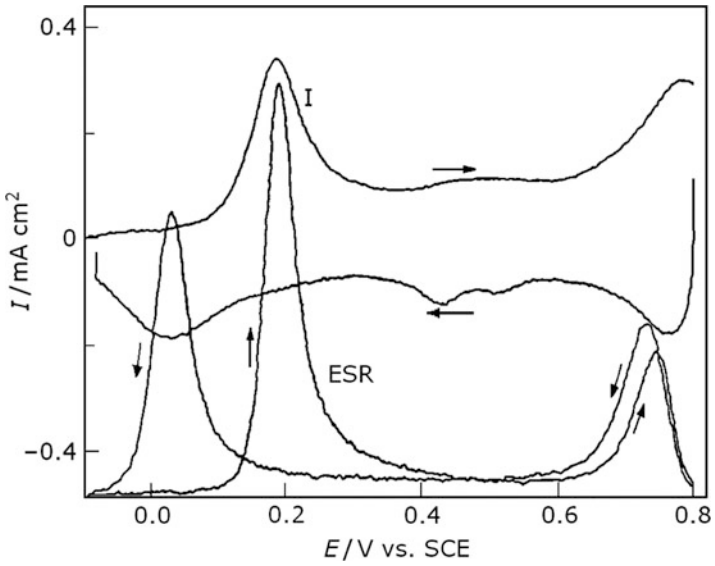

Fig. 6.4 Simultaneous measurements of ESR absorption and current (I) for a 100-nm PANI film on Pt in 0.5 mol dm^{-3} H_2SO_4. The potential was scanned from −0.1 V to +0.8 V and back. Scan rate: 10 mV s^{-1} [69] (Reproduced with the permission of The Electrochemical Society)

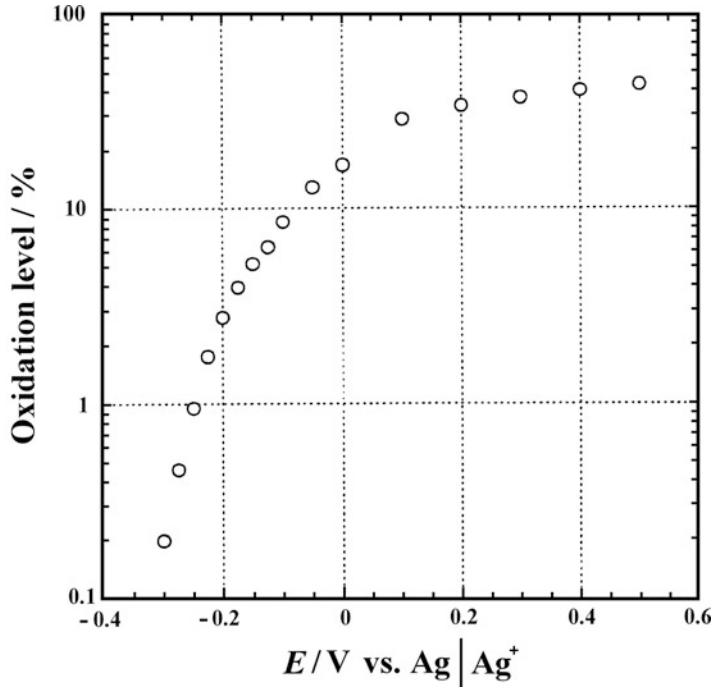

Fig. 6.5 Oxidation levels of the PANI film on Pt as a function of electrode potential. Electrolyte: 0.1 M tetraethylammonium perchlorate (TEAP) in acetonitrile (Reproduced from [78] with the permission of Elsevier Ltd.)

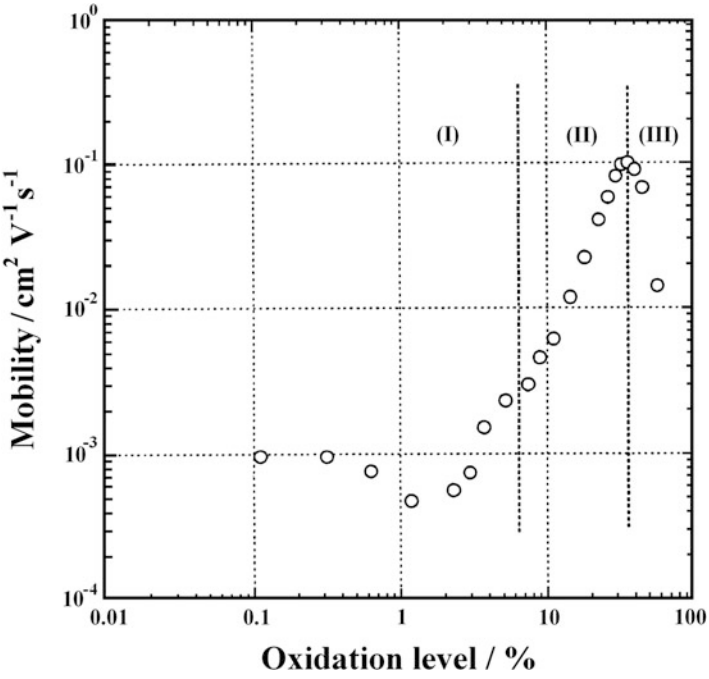

Fig. 6.6 Mobilities of positive charge carriers in the PANI film at different oxidation levels. Electrolyte: 0.1 M tetraethylammonium perchlorate (TEAP) in acetonitrile (Reproduced from [78] with the permission of Elsevier Ltd.)

higher charging levels is due to the transformation between Curie spins (unpaired electrons are localized or poorly delocalized) and Pauli spins (unpaired electrons are delocalized in a conduction band). (As well as the number of spins, the linewidth, and the g-factor as a function of the oxidation level have also been analyzed.) The optical spectra indicate that the small mobility decrease during the early phase of oxidation can be ascribed to a change in the polymer conformation from a simple coil to an expanded coil [78].

Various models have been developed to explain the mechanism of charge transport in conducting polymer film electrodes. Two extreme approaches exist. According to the delocalized band model, the charges and unpaired electrons are delocalized over a large number of monomer units [57, 69, 79, 80], while in the chemical model the charge is localized in the polymer chain [75], or at most only some monomer units are involved. The approach assuming localized charges does not differ essentially from that applied for redox polymers. Therefore, we will deal with the semiconductor or one-dimensional metal models [48, 51, 81] herein. Although the precise nature of charge carriers in conjugated systems varies from material to material, in general the following delocalized defects are considered: solitons (neutral defect state), polarons (a neutral and a charged soliton in the same chain, which are essentially singly charged cation radicals at the polymer chain coupled with local deformations), and bipolarons

(two charged defects form a pair; these doubly oxidized, spinless dications usually exist at higher charging levels) [48, 68, 82–89].

The macroscopic charge transport in a conducting polymer matrix represents a superposition of the local transport mechanism. The intrinsic conductivity, which refers to the conduction process along a conjugated chain, can be described in terms of band theory, which is well established for solid materials. Metallic conductors are characterized by either a partially filled valence band or an overlap between the valence and conduction bands. Semiconductors and insulators possess a band gap between the top of the valence band and the bottom of the conduction band. The band gap energy is relatively small for a semiconductor but rather large for an insulator. The neutral (reduced, undoped) polymer has a full valence and empty conduction band separated by a band gap (insulator).

Chemical or electrochemical doping (oxidation and incorporation of counterions) results in the generation of a polaron level at midgap. Further oxidation leads to the formation of bipolaron energy bands in the band gap. Electronic conductivity is rationalized in terms of bipolaron hopping. Because the overall size of the polymer is limited, interchain electron transfer must also be considered. The intrachain conductivity of the polymer is usually very high if the polymer chain is long and contains no defects; therefore, the interchain conductivity is rate determining in a good-quality polymer [83]. (If the polymer morphology is fibrillar, the fiber-to-fiber electron transport may also be the most hindered process.) The essential aim is to synthesize conducting polymers where the mean free path is limited by intrinsic scattering events from the thermal vibrations of the lattice (phonons). One of the problems is that quasi-one-dimensional electronic systems are prone to localization of electronic states due to disorder. In the case of electronic localization, the carrier transport is limited by phonon-assisted hopping, according to the Mott model [90]. The Mott model of variable range hopping gives the following equation for the conductivity (σ):

$$\sigma = \sigma_0 \exp\left[-\left(\frac{T_0}{T}\right)^{\gamma}\right], \tag{6.15}$$

where σ_0 and T_0 are constants and γ is a number related to the dimensionality (d) of the hopping process ($\gamma = (d + 1)^{-1}$).

The σ_0 value depends on the electron–phonon coupling constant, while T_0 is connected to the localized density of states near the Fermi level and the decay length of the wavefunction. It can be seen that conductivity increases with temperature, in contrast to the situation for metals. This type of conductive behavior has been verified for many conjugated polymer systems. The problem of localization is less important if the molar mass of the polymer is high and only a few defects are present, and a relatively intense interchain coupling prevails. In this case, the mean free path becomes quite large and is determined by phonon scattering, as in true metals. Under such conditions, the conductivity is high, and its value increases with the molar mass of the polymer and decreases with the temperature.

The mechanism of fluctuation-induced tunneling is expected for the electrical conductivity if large regions of a highly conductive ("metallic") phase in an inhomogeneous material are separated from each other by an insulating phase. The latter acts as a potential barrier. Due to the exponential dependence of the tunneling probability, tunneling will effectively occur only in the regions of closest approach of the metallic segments.

The parabolic barrier approximation for the fluctuation-induced tunneling gives the following relationship in terms of the temperature dependence of conductivity [85, 91]:

$$\sigma = \sigma_0 \ \exp\left[-\frac{T_1}{T - T_0}\right], \tag{6.16}$$

where the parameters T_1 and T_0 are associated with the parameters of the tunnel junction (its effective area, width, the height of the potential barrier, its effective mass and dielectric permittivity). For instance, the temperature dependence of the conductivity of polypyrrole has been analyzed using this theory. On the basis of this analysis, an interesting conclusion has been drawn about the structure of the polymer, namely that the polymer consists of islands with two-dimensional (macrocyclic) structure which are connected (cross-linked) by one-dimensional polypyrrole chains [92].

The conductivity may depend on other factors; for instance on the pH of the contacting solution (proton doping in the case of polyaniline) (Fig. 6.7) or on the presence of electron donor molecules in the gas phase.

Decreasing the pH of the solution increases the conductivity of polyaniline [54, 79, 93], while the resistance of dry polyaniline (Fig. 6.8) and polypyrrole increases in an ammonia atmosphere [94, 95].

Electron-conducting polymers can easily be switched between conducting and insulating states just by changing the potential, by electrochemical (or chemical) oxidation and reduction, respectively, or by varying the composition of the contacting fluid media (H^+ ion activity of the solution, or the NH_3 [96, 97], NO, etc., concentration in the gas phase). The variation in the resistance of polyaniline as a function of potential nicely demonstrates the conversion from the insulating to the conducting state and vice versa (Fig. 6.9).

This is a unique property in comparison with the majority of electron-conducting materials (e.g., metals). When the oxidation state of the polymers is varied, not just their conductivity but other properties change too (e.g., color). It is this feature that can be exploited in many practical applications [1, 98] (see Chap. 7).

Figure 6.10 shows the spectra of a PANI film measured in situ at different potentials [99]. The absorption maximum at 310–320 nm is characteristic of the reduced diamagnetic initial state (leucoemeraldine structure), and this band decreases during the oxidation of PANI. The band at 420–440 nm can be assigned to the paramagnetic polaronic/radical cation state. This band appears in the first phase of oxidation simultaneously with the increasing absorbance in the region

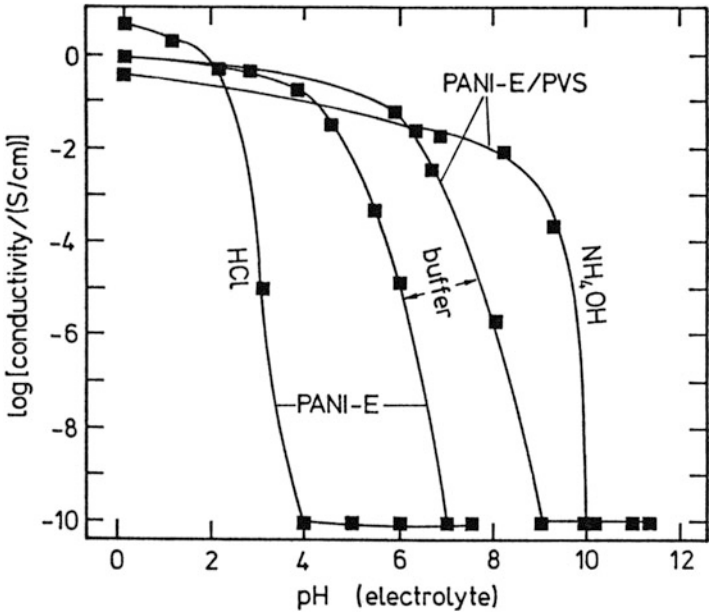

Fig. 6.7 The conductivity of PANI in emeraldine state (PANI-E) with and without poly (vinylsulfonate) (PVS) incorporated into the polymer matrix, as a function of the composition of the electrolyte with which the polymer was equilibrated. PANI-E + buffer: 0.05 M $C_6H_4(COO^-)_2$ plus appropriate amounts of HCl or NaOH [The concentration of the exchanging anionic species, $C_6H_4(COO^-)_2$, is about ten times higher in the film than in the solution.]. PANI-E/PVS + buffer: 0.05 M phosphoric or boric acid plus appropriate amounts of NaOH [53]

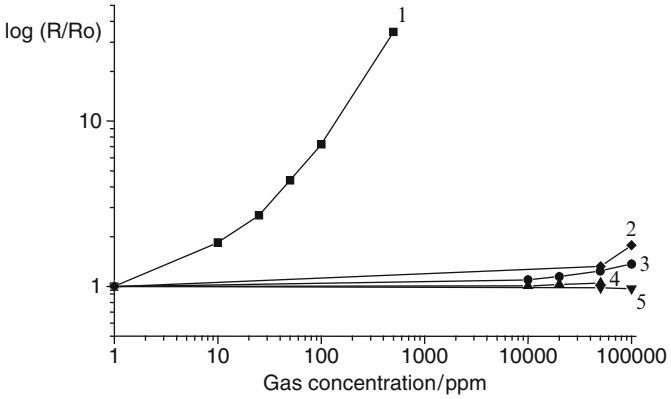

Fig. 6.8 The response of a PANI ammonia sensor (log relative resistance–gas concentration plot) for different gases and vapors: (*1*) ammonia; (*2*) methanol; (*3*) ethanol; (*4*) CO; and (*5*) NO, at room temperature [96]

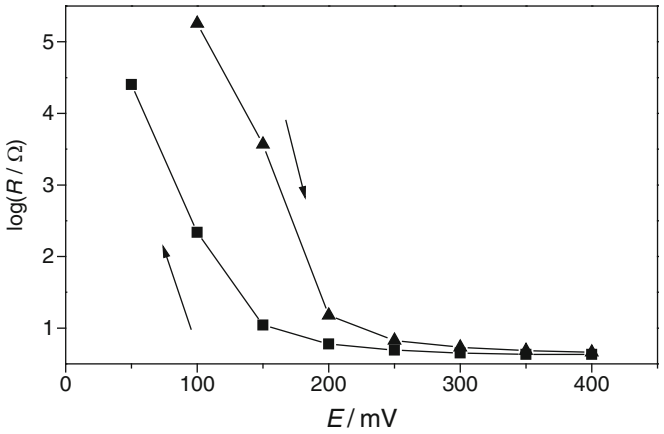

Fig. 6.9 The change in the resistance of a polyaniline film in contact with 1 M H_2SO_4 as a function of the potential (Reproduced from [97] with the permission of Elsevier Ltd.)

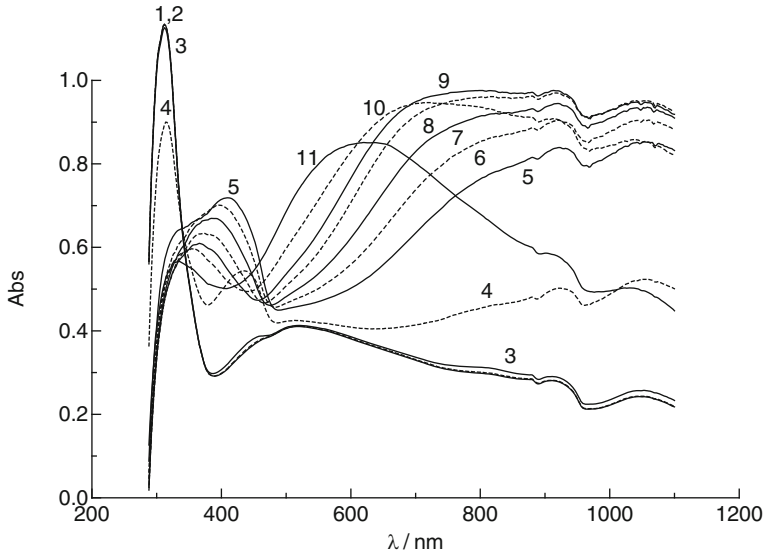

Fig. 6.10 In situ UV–VIS–NIR spectra of a PANI film obtained at different potentials: (*1*) −0.35; (*2*) −0.25; (*3*) −0.15; (*4*) −0.05; (*5*) 0.05; (*6*) 0.15; (*7*) 0.25; (*8*) 0.35; (*9*) 0.45; (*10*) 0.55; and (*11*) 0.65 V vs. SCE. Solution: 1 mol dm^{-3} H_2SO_4 (Reproduced from [99] with the permission of Elsevier Ltd.)

$\lambda > 600$ nm. The latter absorption is a characteristic feature of all electronically conducting polymers, and it is connected with the conversion of localized redox centers into delocalized free electron states (electron transfer from the valence band to the polaron–bipolaron levels). At higher potentials, the absorption

band at ca. 430 nm (which reaches its highest value at the beginning of the anodic voltammetric wave) decreases, and a blue shift can also be observed, attesting a further transformation in the form of the radical and an interplay between the benzenoid (leucoemeraldine) and quinoid structures with better π-conjugation (emeraldine form).

A conformational change and intermolecular stabilization [71] as well as dimerization and disproportion of polaronic segments [100] have also been proposed in order to explain the behavior in this potential region. The absorbance related to the delocalized electrons increases also in the so-called capacitive region; then, as the polymer becomes fully oxidized (the pernigraniline structure is formed) in the region of the second voltammetric wave, the free electron band gradually disappears and a new band appears at ca. 610 nm. The vibrational spectra also change during the redox transformations of conducting polymers. The results from in situ FTIR-ATR measurements [101] are presented in Fig. 6.11. At pH 1 the absorption intensities detected for a PANI electrode at 1,564, 1,481, 1,304, 1,250, 1,144 (semiquinoid ring vibrations), 889, 822, and 802 cm^{-1} increase, while absorption at 1,502 cm^{-1} (assigned to a benzoid ring mode) and 1,203 cm^{-1} decreases with increasing potential. At pH 4, a band shift is detectable (1,564 → 1,576, 1,481 → 1,487, 1,144 → 1,136, and 822 → 831 cm^{-1}) and some additional bands appear at 1,375, 1,184, and 864 cm^{-1} [101]. The occurrence of the CH (out-of-plane) vibrational band at 831–822 cm^{-1} can be attributed to a semiquinoid polaron lattice structure. The bands appearing at 1,375 and 864 cm^{-1} at pH 4 can be assigned to a ring-N-ring vibration in the quinoid form and to a C–H (out-of-plane) mode, respectively, and those indicate the transition from the polaron to a bipolaron lattice structure with completely quinoid rings. At low pH values, the background absorption increases due to the high electrical conduction. The 889 cm^{-1} band is due to the inserted ReO_4^- anions [101].

Charging/discharging (or redox switching) processes are usually fast, but are rather complex in nature. The steady-state cyclic voltammograms exhibit in most cases a combination of broad anodic and cathodic peaks with a plateau in the current at higher potentials. This is illustrated in Fig. 6.12.

The current is proportional to the scan rate, i.e., from an electrical point of view the film behaves like a capacitor [102–108]. However, this simple result is the consequence of a complicated phenomenon which includes a faradaic process (the generation of charged electronic entities at the polymer chains near the electrode surface by electron transfer to the metal), the transport of those species throughout the film, as well as the ion exchange at the film–solution interface (see mass changes during charging/discharging cycles in Fig. 6.12).

Despite the above-mentioned quasi-equilibrium character of the cyclic voltammetric curves, a pronounced hysteresis (i.e., a considerable difference between the anodic and cathodic peak potentials) appears. Slow heterogeneous electron transfer, effects of local rearrangements of polymer chains, slow mutual transformations of various electronic species, a first-order phase transition due to an S-shaped energy diagram (e.g., due to attractive interactions between the electronic and ionic charges), dimerization, and insufficient conductivity of the film at the beginning

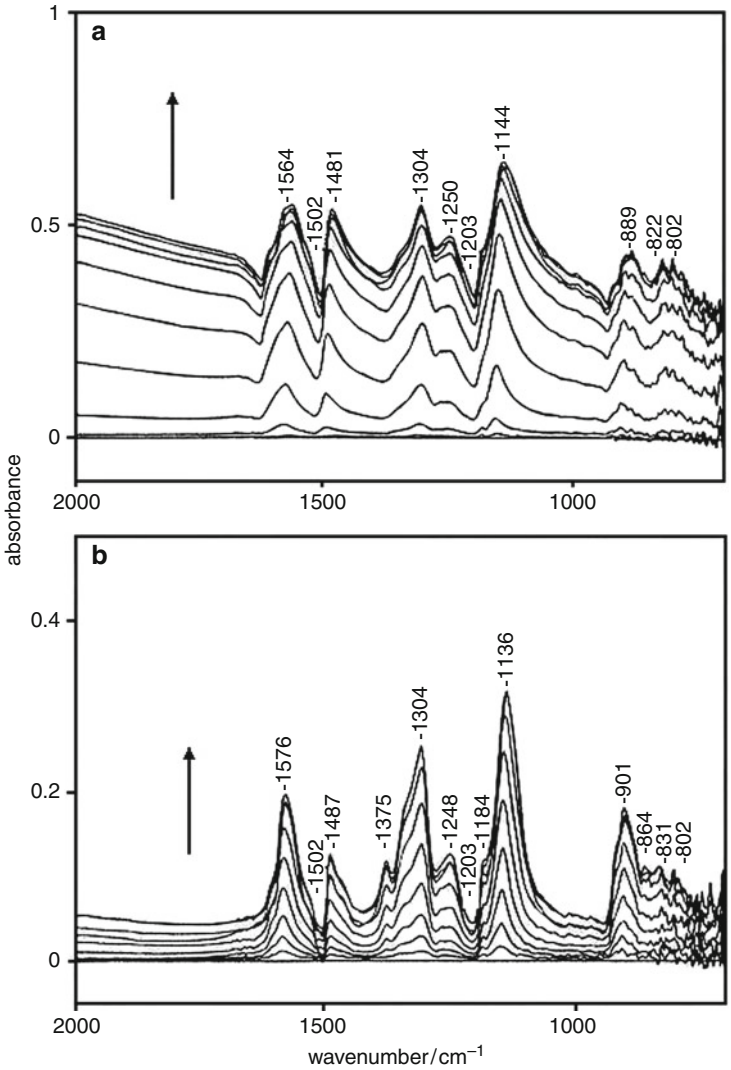

Fig. 6.11 Changes in the FTIR-ATR spectra of PANI obtained during a potential sweep ($v = 1$ mV s^{-1}) in $HReO_4$–$NaReO_4$ electrolyte; potential range: −200 to 400 mV. Reference state: fully reduced form (−200 mV). Each spectrum covers 40 mV. (**a**) pH 1; (**b**) pH 4. The *arrow* indicates the direction of increasing potential (Reproduced from [101] with the permission of The Royal Society of Chemistry)

of the anodic process have been proposed as possible explanations for the hysteresis [71, 100, 109–114] (See also Sect. 6.6).

In polymers which have an electron-conducting backbone with pendant or built-in redox groups (e.g., conjugated metallopolymers), three electron transfer pathways may be operative [115] (see Fig. 6.13).

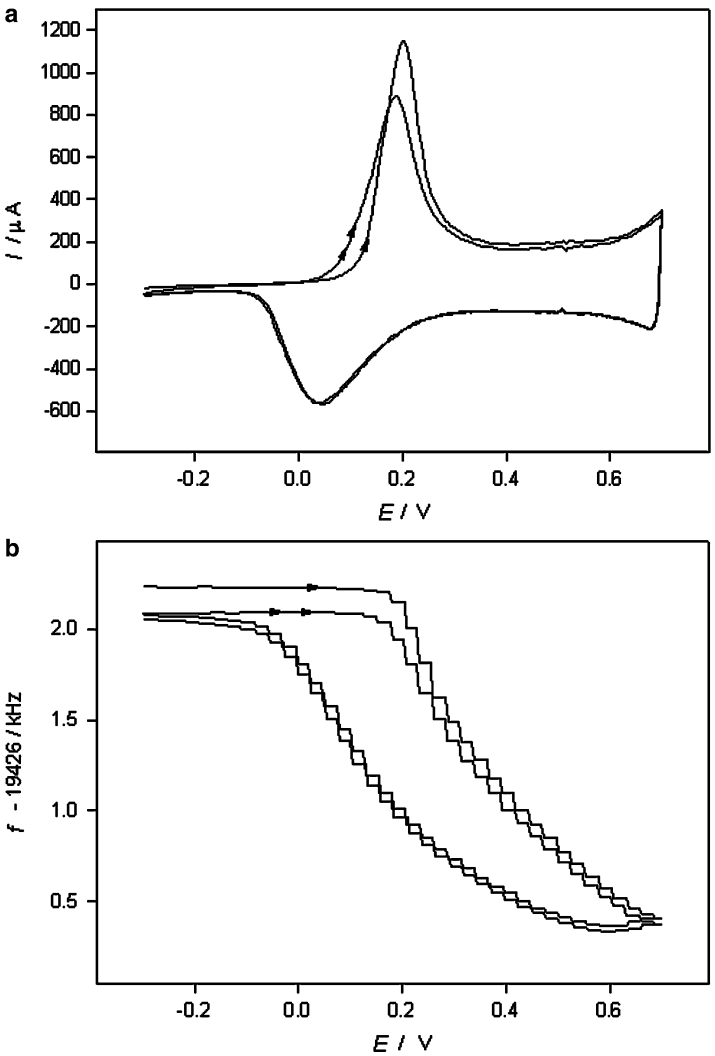

Fig. 6.12 Cyclic voltammograms (two cycles; **a**) and (**b**) the simultaneously detected EQCN frequency changes for a polyaniline film ($L = 2.9$ μm) in contact with 1 M H_2SO_4. Sweep rate: 100 mV s^{-1} (Reproduced from [97] with the permission of Elsevier Ltd.)

There is electron hopping between the redox centers (process 1), as in conventional redox polymers. Electron transfer may also occur through the polymer backbone via a metal–metal electronic interaction (process 2, superexchange pathway) or via polymer-based charge carriers (process 3, polymer mediation). The electronic interactions between the π-system of the polymer and the *d*-orbitals of the metal centers usually enhance the rate of the electron transfer process. Electron transfer via polymer-based charge carriers requires the polymer to be electronically

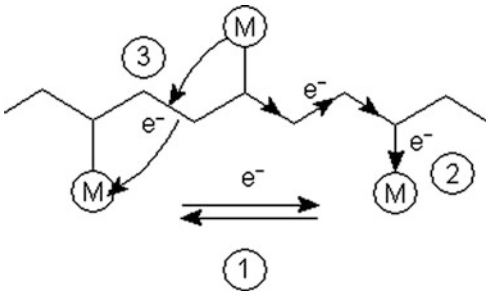

Fig. 6.13 Illustration of the three electron transfer pathways between metal centers in which the electron-conducting polymer backbone participates: (*1*) electron transfer reaction (outer sphere electron transfer; (*2*) superexchange pathway; (*3*) polymer-mediated pathway

conductive at potentials close to the formal potential of the redox groups. An increased electron transport, mediated through the conducting polymer backbone, significantly enhanced the electrochemiluminescence efficiency in polyaniline or polypyrrole/$Os(bpy)_3^{3+/2+}$ system [116].

6.2 Ion Transport

During electrochemical oxidation or reduction of the surface polymer films or membranes, the overall electroneutrality of the polymer phase is retained due to ion exchange processes between the polymer film and the bulk electrolyte solution [2, 117–119]. Beside solvent and other neutral molecules may enter or leave the film during the charging/discharging processes [2–4, 6, 23, 120–124]. In order to maintain electroneutrality in the simplest case, either counterions must enter the film or co-ions must leave it. (Co-ions are ions of the electrolyte present in the film which have the same charge as the redox sites created by the electron transfer reaction.) The relative contributions of ions carrying different charges to the overall charge transport may depend on their physical properties (e.g., size) and/or on their chemical nature (e.g., specific interactions with the polymer), as well as on other parameters (e.g., potential) [2–4, 6, 19, 22, 23, 120–177].

There are a wide range of reaction schemes; however, most of the redox transformations that include the participation of mobile ions of the contacting electrolyte can be represented as follows:

Reduction.

$$P + e^- + M^+ \rightleftarrows P^{\bullet -} M^+, \tag{6.17}$$

$$P^{\bullet -} M^+ + e^- + M^+ \rightleftarrows P^{2-} M_2^+. \tag{6.18}$$

Dimerization and protonation may also occur:

$$P + P^{\bullet -} M^+ \rightleftarrows P_2^{\bullet -} M^+, \tag{6.19}$$

$$2P^{\bullet -}M^{+} \rightleftarrows P_2^{2-}M_2^{+}, \tag{6.20}$$

$$P^{\bullet -}M^{+} + e^{-} + H^{+} \rightleftarrows PH^{-}M^{+}, \tag{6.21}$$

$$P + 2e^{-} + 2H^{+} \rightleftarrows PH_2, \tag{6.22}$$

where P is a polymer with reducible groups and M^+ is the counterion (cation). A typical example of such a polymer is poly(tetracyanoquinodimethane) [2, 126–128, 135]; however, the behaviors of electronically conducting polymers [e.g., the cyclic voltammetric responses of poly(*p*-phenylene)] have also been elucidated by a dimerization scheme [114]. For organic redox or conducting polymers, the nine-member square scheme elaborated for the electrochemical transformation of quinones can be applied partially or wholly, because electron transfer is always coupled with protonation depending on the pH of the contacting solutions.

Oxidation.

$$P + X^{-} \rightleftarrows P^{+}X^{-} + e^{-}, \tag{6.23}$$

where X^- is a counterion (anion) (Examples: polyvinylferrocene [128, 136, 150] or poly[$Os^{(II)}(bpy)_2(vpy)_2$] X_2^- [138].)

$$P + X^{-} \rightleftarrows P^{+\bullet}X^{-} + e^{-}, \tag{6.24}$$

$$P^{+\bullet}X^{-} + X^{-} \rightleftarrows P^{2+}X_2^{-} + e^{-}. \tag{6.25}$$

(Examples: poly(tetrathiafulvalene); dimeric species are also formed [129, 138].)

In reactions (6.17)–(6.25), cations (M^+ or H^+) and anions (X^-) enter the film during reduction and oxidation, respectively. In some cases, cations (i.e., the co-ions) leave the polymer film during oxidation:

$$M_2^{+}[A(II)B(II)L_6]^{2-} \rightleftarrows M^{+}[A(II)B(III)L_6]^{-} + M^{+}, \tag{6.26}$$

$$PP - SO_3^{-}M^{+} \rightleftarrows PP^{+}SO_3^{-} + M^{+} + e^{-}. \tag{6.27}$$

(Examples: $K_2^+[Ni(II)Fe(II)(CN)_6]$ [134] or self-doped polypyrrole [140–143] or polyaniline, see the scheme in Sect. 2.2.1.1, or poly(diphenylamine), see Sect. 2.2.1.2)

The oxidation of organic polymers is often coupled with deprotonation instead of or as well as anion incorporation [2, 109]; see for example the schemes for PANI, poly(diphenylamine), poly(*o*-phenylenediamine), polyphenazine, etc., in Sect. 2.2.

Figure 6.14 shows the cyclic voltammograms and simultaneously detected EQCN responses for PANI electrodes in contact with three different electrolytes

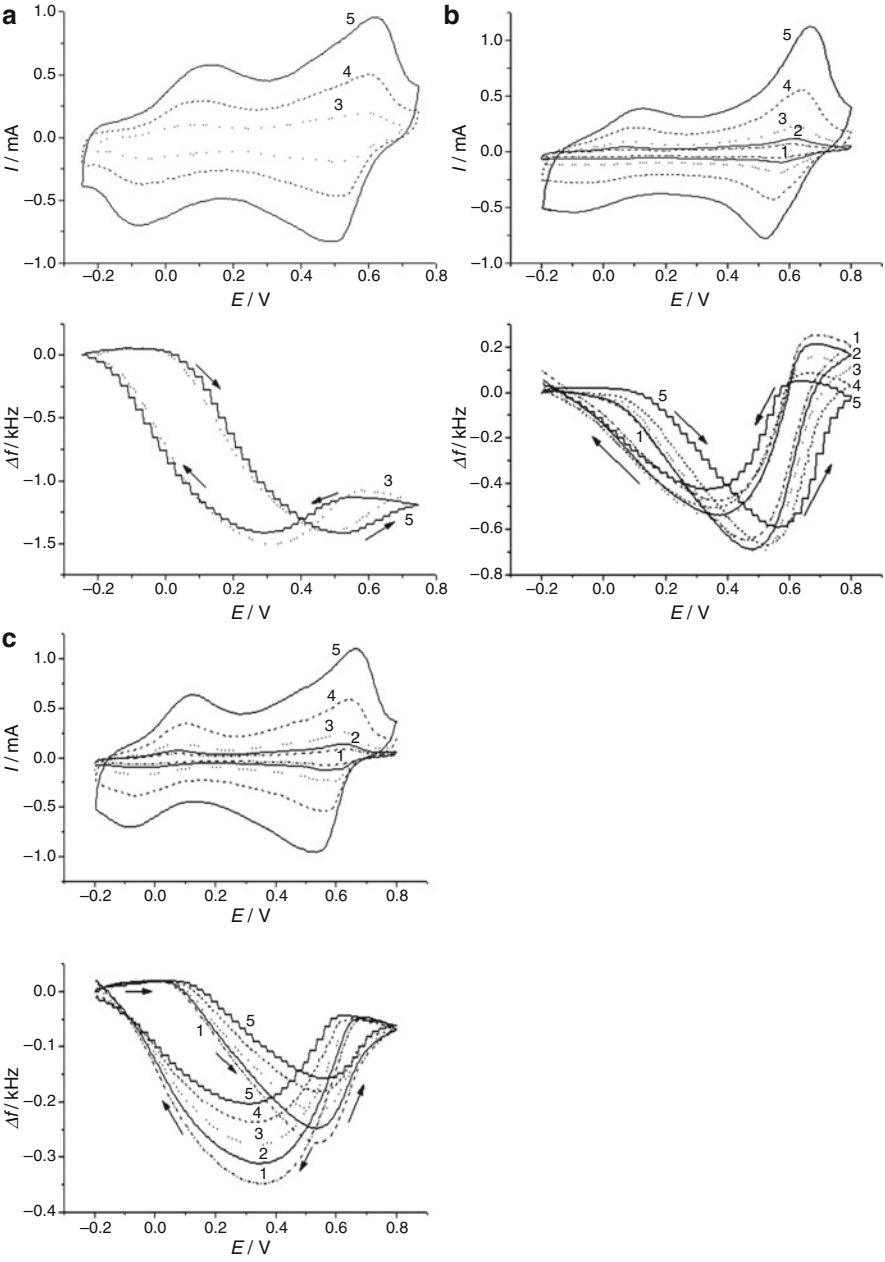

Fig. 6.14 Cyclic voltammograms and simultaneously obtained EQCN frequency changes as a function of scan rate for PANI electrodes in contact with 1 mol dm^{-3} electrolyte containing (**a**) ClO_4^-, (**b**) TSA^-, and (**c**) SSA^- ions, at pH 2. Scan rates are (*1*) 6, (*2*) 10, (*3*) 20, (*4*) 50, and (*5*) 100 mV s^{-1} (TSA^- = 4-toluenesulfonate, SSA^- = 5-sulfosalicylate anions). (Reproduced from [122] with the permission of Elsevier Ltd.)

as a function of the scan rate. Both leucoemeraldine (L) → emeraldine (E or EH_{8x}) and emeraldine → pernigraniline (P) transitions can be seen in the voltammograms. The respective frequency (mass) changes reveal that at pH 2 the dominant reaction path is L → EH_{8x} → P (see the scheme given in Sect. 2.2.1.1). (At pH 2 the rate of the hydrolysis of pernigraniline is slow, and consequently the E (or EH_{8x}) → P transition can also be studied without any deterioration of the polymer. It may also help that at pH 2 the voltammetric wave appears at a less positive potential, since the pH dependence of these peaks is −120 mV/pH). These curves show several very interesting features. First, it is evident that the relative contribution of protons (hydronium ions) to charge transport is still substantial during the early phase of oxidation; i.e., some of the leucoemeraldine is still protonated (LH_{8x}) and/or unprotonated emeraldine (E) also forms. It is understandable that this effect is more pronounced at lower pH values, which is clearly apparent in Fig. 6.12. At pH 0, the mass change is minor, although a substantial amount of charge has already been injected. The low mass change is due to the low molar mass of H^+ ion, which is the species that leaves the surface layer. The incorporation of the anions, which have a much higher molar mass, clearly manifests itself in the observed EQCN frequency decrease [122, 144]. Simultaneous proton–anion exchange can also be detected by a probe beam deflection technique. Figure 6.15 shows the cyclic voltammogram and the simultaneously obtained voltadeflectogram for a PANI film in 1 mol dm^{-3} $HClO_4$ [130, 145].

The small negative deflection pre-peak is due to the dehydrogenation and expulsion of protons in the region of the first voltammetric oxidation peak. This is followed by a large positive deflection peak which indicates anion insertion. During the second oxidation process, where emeraldine → pernigraniline transformations occur, both proton and anion expulsions take place (see the scheme in Sect. 2.2.1.1), which are indicated by the negative deflection. In the reduction scan, the opposite behavior is exhibited.

Theoretical calculation based on a polaronic model [147] elaborated by Daikhin and Levi may give an explanation for the separation of the proton and anion transports. In this model, Coulomb interactions between species with opposite signs have been taken into account. Owing to the very high repulsion forces between the nearest neighbor sites in the polymer chain, it is unfavorable that protons on the nitrogen atom and the benzenoid ring filled with a hole (polaron) should exist next to each other simultaneously. Consequently, deprotonation is a necessary process when positive charges are injected into the polymer. This provides an explanation for the deprotonation reaction that occurs at low potentials and also resolves the apparent contradiction between experimental results and the consequences of applying the classical square scheme for coupled electron and proton transfer steps, because the latter predicts that unprotonated leucoemeraldine can be oxidized at less positive potentials than the protonated one. Second, the sweep rate dependence of the EQCN response indicates that, in both redox steps, completion of the sorption/desorption processes depends on the time scale of the experiment in a similar manner. Third, the ratio of peak currents for the first and second waves increases in the order $ClO_4^- < SSA^- < TSA^-$ (SSA^- = 5-sulfosalicylate anions,

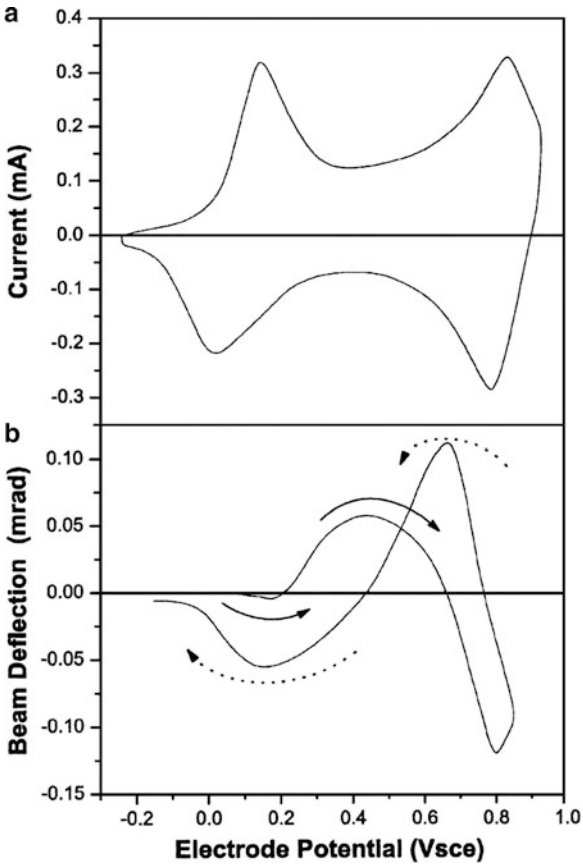

Fig. 6.15 Cyclic voltammogram (**a**) and voltadeflectogram (**b**) of a PANI film in 1 mol dm^{-3} $HClO_4$. Scan rate: 50 mV s^{-1}. Forward scan (*full arrow*) and backward scan (*dotted arrow*) are shown (Reproduced from [146] with the permission of Elsevier Ltd.)

TSA^- = 4-toluenesulfonate anions), and a similar proportionality holds for the mass change that occurs simultaneously. A detailed discussion of the results presented in Fig. 6.14, including solvent sorption and hysteretic behavior, can be found in [122].

The thin-layer STM technique enables a sensitive semiquantitative local study of the H^+ exchange processes associated with the redox transformations of PANI [148]. It was found that at pH 2 significant H^+ exchange only occurs during the emeraldine $\rightleftarrows$ pernigraniline transition.

The proton concentration at the PANI–electrolyte interface was monitored by scanning electrochemical microscopy during the redox reactions of the polymer. These experiments provided direct evidence of the increased protonation of the leucoemeraldine form as the concentration of added NaCl is increased [149].

The results obtained by different techniques (radiotracer [123, 128], quartz crystal nanobalance [22, 120–122, 124–126, 132–134, 150–164], probe beam deflection [130, 133, 145, 166], STM [148], SECM [149], etc.) have revealed that the situation may be even more complicated than this. It has been found that the

relative contributions of anions and cations to the overall ionic charge transport process depend upon several factors, such as the oxidation state of the polymer (potential), the composition of the supporting electrolyte, and the film thickness [2, 19, 22, 23, 120–134, 150, 152, 164, 168]. The latter effect is shown in Fig. 6.16.

These phenomena can be understood in terms of morphological changes, ion mobilities, interactions between the polymer and the mobile species (ions and solvent molecules), size exclusion, and so forth [19, 22, 23, 61, 78, 120–134, 150, 153–175].

For instance, if large counterions are used during film deposition (electropolymerization), co-ion exchange is largely observed. In this case, the large, sometimes polymeric counterions are trapped in the polymeric layer due to strong van der Waals and electrostatic forces.

The charge transport diffusion coefficient, which can be determined by transient techniques, is characteristic of the rate-limiting step (either the electron or the ionic charge transport). However, it is possible to decouple the electron and ion transport using appropriate experimental techniques, and so the rates of the fundamental charge transport processes can be determined separately.

The transport of ionic species can be described using the Nernst–Planck equation. In the absence of a mediated reaction, the convection term can be omitted, because any stirring of the solution has no effect inside the film. At high concentrations, the fluxes have a more complicated form due to the upper limits on concentrations and/or short-range interactions between the species. Because of the nonlinear character of the resulting equations, the solutions are usually obtained using various approximations. The Poisson equation is usually replaced by the local electroneutrality condition; this is justified for a sufficiently large ratio of the film thickness to its Debye screening length and for a slow variation in potential. In the presence of excess supporting electrolyte, the contribution to the flux from migration may also be neglected. Diffusion–migration transport equations have mostly been solved for one-dimensional transport [2–4, 176, 177].

6.3 Coupling of Electron and Ionic Charge Transport

The electronic and ionic charge transport processes are coupled by the electroneutrality condition. This statement is valid for systems with different structures (e.g., uniform and porous films) as well as for different mechanisms of electronic charge transport (e.g., electron hopping between redox centers, migration–diffusion transport of an incorporated electroactive component across the film, or long-distance movement of charged sites in the matrix); however, each case needs somewhat different theoretical treatments and the experimental manifestation (e.g., in the steady-state or transient current) of this effect depends on other factors (e.g., on the concentration of background electrolyte and the charge of the polymer) [13–16, 41–44, 178–195]. Typically, two mobile species are considered, assuming that a Donnan exclusion exists (i.e., that co-ions do not participate in the charge

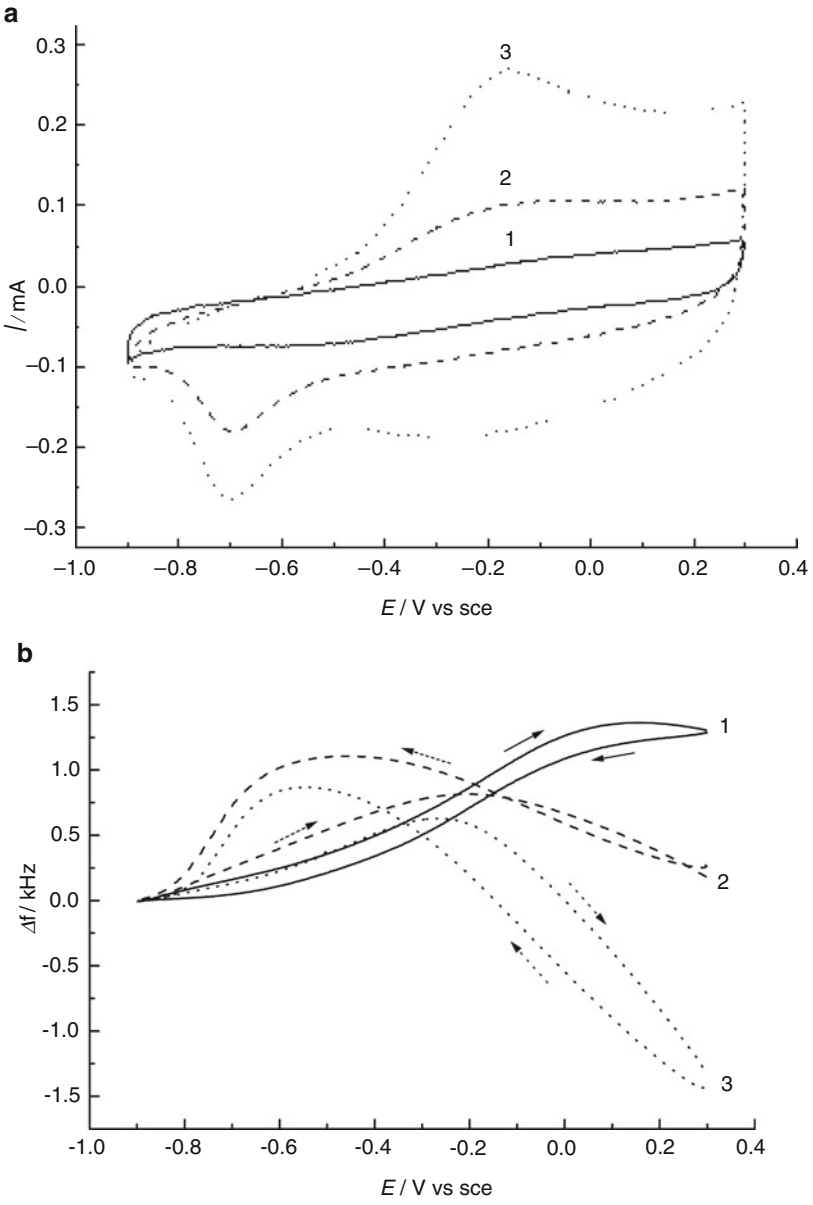

Fig. 6.16 Effect of the thickness on the cyclic voltammetric (**a**) and EQCN (**b**) responses of polypyrrole films. The thicknesses are (*1*) 0.14, (*2*) 0.48, and (*3*) 0.96 μm, respectively. Solution: 1 M NaCl; $v = 10$ mV s^{-1} [124] (Reproduced with the permission of Springer-Verlag)

transport). However, a theoretical model involving a diffusion and migration charge transport mechanism with three charge carriers has also been developed [179]. It is a fundamental feature of all these analyses that electron transport is not only driven

by a concentration gradient, but that migration plays also a role. It was recognized that the electron hopping process cannot be described by the usual combination of the classical Fick and Nernst–Planck laws, where the effect of the electric field is considered, but rather a second-order law should be derived from the bimolecular character of electron hopping, as opposed to the unimolecular character of ion displacement [13–16, 41–44]. For systems in which the ratio of the oxidized and reduced forms is fixed and kept constant (i.e., the total charge of the redox species and hence the concentration of counterions are fixed), the theory predicts a maximum in the steady-state current (redox conductivity) near the formal potential of the redox couple. The current due to the electron hopping is higher than that which occurs in the absence of migration.

A detailed analysis of the modified Nernst–Planck equation derived from the diffusion–migration model for coupled transport of the electronic and ionic charge carriers indicates that under both steady-state and transient conditions, migration always leads to an enhancement of intersite electron hopping, and somewhat surprisingly the enhancement increases as the mobility of the counterions decreases. Migration diminishes in all cases as the relative concentration of electroactive fixed counterions is increased (i.e., the fixed counterions play a role similar to that of the supporting electrolyte in solution studies). This is especially true when the diffusion coefficient of the mobile counterions is small compared to the diffusion coefficient for electron hopping. Another important result of this theory is that the charge transport diffusion coefficient, which can be determined by chronoamperometry, increases with the concentration of the redox species more rapidly than predicted by the Dahms–Ruff equation [11, 26, 46]. (D varies as c^2 or even c^3.)

The data obtained for $Ru(bpy)_3^{3+/2+}$ illustrates such a situation. Based on the results from potential step chronoamperospectrometry, Kaneko et al. concluded that the oxidation of $Ru(bpy)_3^{2}$ to $Ru(bpy)_3^{3+}$ in Nafion films takes place via electron hopping, but physical diffusion plays a key role in the reduction [196], which is in accordance with earlier findings [2].

The electron transfer distance, which includes the physical vibration of the redox species around its anchoring position (called bounded motion [26]) and the distance of the electron exchange reaction, increases as a function of potential due to the increase in the center-to-center distance, which is 1.13 nm at 1.1 V and 1.47 nm at 1.5 V vs. SCE. The bounded motion distance, which is estimated as 0.25–0.31 nm, remains unchanged.

The bimolecular rate coefficient of the electron transfer reaction (k_e) also increases with increasing potential. The apparent diffusion coefficient (D_{app}) for the reduction is higher than that measured for the oxidation. The relationship between k_e and D_{app} is

$$D_{app} = \frac{k_e c(\delta^2 + n\lambda^2)}{6}, \tag{6.28}$$

where, as well as the electron hopping distance (δ), the bounded motion distance (λ) is taken into account, and n is the dimension of the charge transfer, which equals 3 in this case. Equation (6.28) predicts a linear D_{app} vs. c function; however, as seen

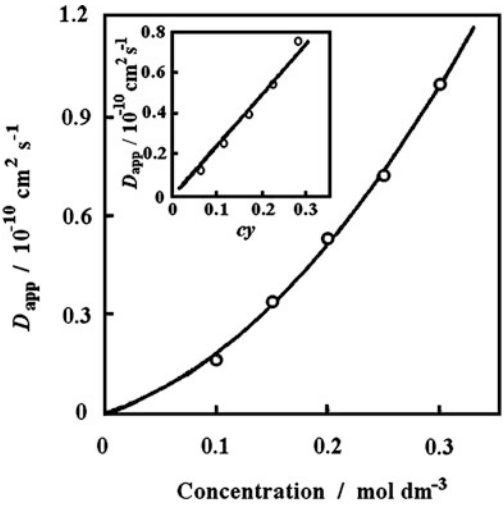

Fig. 6.17 The apparent diffusion coefficient of charge transport (D_{app}) obtained by chronoamperospectrometry as a function of the concentration of the Ru $(bpy)_3^{2+}$ species (c) in a Nafion film. The *inset* shows the D_{app} vs. c_y function, where y is the electrochemically active fraction determined from optical absorbance (Reproduced from [196] with the permission of Elsevier Ltd.)

in Fig. 6.17, a faster rise in D_{app} can be observed at higher concentrations. This was explained by the increasing participation of the redox sites in the oxidation process; i.e., at low concentrations many isolated clusters exist, and electrons are not transported to these by hopping.

An exponential decrease in the rate coefficient of the electron transfer (k_e) as a function of the distance was assumed. As can be seen in Fig. 6.18, the rate coefficient corresponding to the redox complexes in close contact (k_o) increases strongly with the potential, so increasing the electric field enhances both the electron hopping distance and the electron propagation rate [42, 43].

The increase in the rate of electron transfer was assigned to the enhancement of the counterion migration rate [196]. The rate of the reduction increased linearly with the redox center concentration, while D_{app} was independent of c, which indicates that a diffusion mechanism prevails.

It was concluded that the strength of the electrostatic interactions between $Ru(bpy)_3^{2+}$ and $Ru(bpy)_3^{3+}$ and the sulfonic anions in Nafion plays a key role. Since the electrostatic interaction is weaker in the case of $Ru(bpy)_3^{2+}$, the motions of these ions are less hindered, and so their physical diffusion can contribute to charge propagation during reduction. In contrast with reduction, the products of oxidation, i.e., $Ru(bpy)_3^{3+}$ ions, form strong cross-links with the anionic groups of Nafion, and the charge transfer takes place by electron hopping.

The charge propagation in layer by layer (LbL) electrostatically self-assembled redox polyelectrolyte multilayers has been studied experimentally and theoretically by Calvo et al. by using cationic osmium pyridine–bipyridine derivatized poly(allylamine) and poly(vinyl sulfonate) polyanion model system in different electrolytes [197, 198]. The dramatic effects of outmost layer were emphasized. A diffusion model was developed to account for the experimentally observed dependence of the average peak potential with the scan rate. This model was able to describe both the redox peak potential and the current, providing information on the

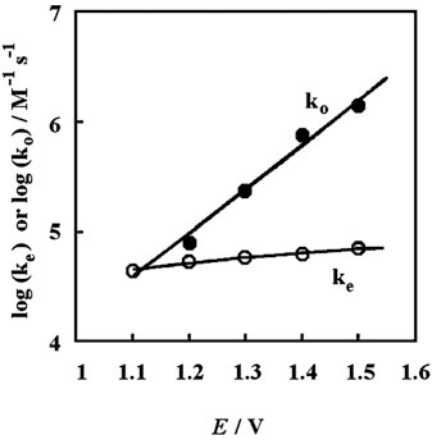

Fig. 6.18 The variations in the bimolecular rate coefficient of the electron transfer reaction (k_e) and the rate coefficient corresponding to the redox complexes in close contact (k_o) as a function of the potential for the $Ru(bpy)_3^{3+/2+}$–Nafion system (Reproduced from [196] with the permission of Elsevier Ltd.)

electron transfer rate constants and the diffusion coefficient for the electron hopping mechanism. The important consequences for electrochemical devices built by layer-by-layer self-assembly, such as amperometric biosensors or electrochromic devices, were also discussed [197, 198]. Besides electric field effects, ion association within the polymer films plays an important role in the dynamics of electron hopping within the films. (Extensive ion association might be expected due to the high ion content and the low dielectric permittivity that prevails in the interiors of many redox polymers.) According to the model that includes ion association, the sharp rise in the apparent diffusion coefficient as the concentration of the redox couple in the film approaches saturation is an expected consequence of the shift in the ionic association equilibrium to produce larger concentrations of the oxidized form of the redox couple, which is related to rapid electron acceptance from the reduced form of the couple [178].

Ion association effects have also been considered in the case of conducting polymers. It is assumed that ions exist inside the polymer films in two different forms.

The bound or immobile ions are associated with either neutral or charged sites in the polymer matrix. Assuming the formation of bonds between the neutral sites and ions, the splitting of the cyclic voltammetric curves and the minimum in the mass versus charge relationship can be explained [186].

The advanced models elaborated for the low-amplitude potential perturbation of metal/conducting polymer film/solution systems also take into account the different mobilities of electronic (polarons) and ionic species within the uniform film. An important feature of this approach is that the difference in the electric and ionic mobilities ($D_e \neq D_i$) leads to nonuniformity of the electric field inside the bulk film, which increases as the ratio D_e/D_i increases, and the electric field will vanish when $D_e = D_i$ [190, 194, 195].

A model was developed, which considers the coupling among electron transfer, deformation, screening, and binding. The model is based on the assumption that macromolecules are composed of segments of different lengths that may bind species present in the contacting solution, which also may contain redox species [199].

6.4 Other Transport Processes

Beside the counterions' sorption/desorption, the exchange of solvent and in some cases that of the salt (acid) molecules between the polymer film and background electrolyte is expected theoretically and has indeed been found experimentally.

6.4.1 Solvent Transport

The equilibrium distribution of neutral molecules depends on the difference between their standard chemical potentials in the polymer and solution phases. The free energy of transfer is higher (i.e., the sorption of neutral molecules in the polymer phase is greater) if the neutral species and the polymer are similar in character [2, 117–119]. For instance, more water will be incorporated into hydrophilic polymers containing polar groups. Because in many cases a neutral polymer is converted into a polyelectrolyte as a function of potential, the partitioning of water between the polymer film and the electrolyte solution will change during the charging/discharging processes. This may cause a swelling or shrinking of the layer. The extent of swelling is strongly affected by the electrolyte composition (both the nature and concentration of the electrolyte) and temperature [2, 19, 120, 124, 126, 200].

The expansion and contraction of the polymer network in conjunction with the sorption/desorption of solvent molecules and ions can be described in terms of mechanical work. This mechanical contribution should be considered in the calculation of the equilibrium electrode potential (see Chap. 5). The deformation coupled to the redox reaction is elastic in nature. A plastic deformation occurs when a neutral, dry film is immersed in electrolyte solution and electrolyzed. It has been observed for a range of neutral polymer films freshly deposited on metal substrates by solvent evaporation techniques that several potential sweeps are required for the films to become fully electroactive [2, 19, 128, 200, 201]. This phenomenon has been referred as the break-in effect (Fig. 6.19).

A secondary break-in effect may be observed when the film is in its neutral form for a long period of time before a repeated charging process. Both break-in effects are attributed to the incorporation of solvent molecules and ions into the film phase during electrolysis, as well as to potential-dependent morphological changes. The rate of the diffusive transport of solvent molecules depends on the structure of the polymer and the motion of polymer segments. In crystalline and cross-linked polymers, or below the glass transition temperature, the movement of the incorporating species may be rather slow. On the other hand, solvent molecules act as plasticizers, and therefore increase the rate of diffusion for both neutral and ionic species inside the film.

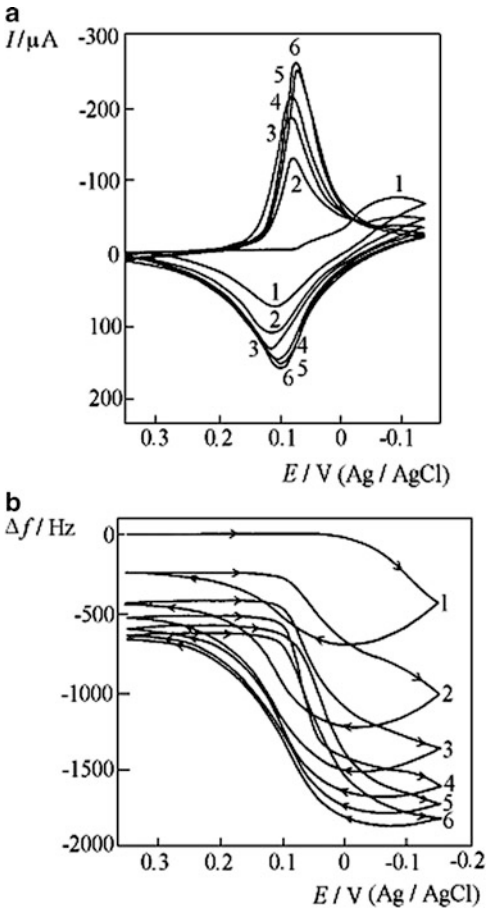

Fig. 6.19 "Break-in effect", as observed in cyclic voltammetric and simultaneous EQCN measurements performed with a poly (tetracyanoquinodimethane) electrode. $\Gamma = 7 \times 10^{-8}$ mol cm^{-2}. Electrolyte: 2.5 M LiCl. Sweep rate: 6 mV s^{-1}. (**a**) Consecutive cyclic voltammograms; (**b**) simultaneously obtained EQCM frequency curves (Reproduced from [200] with the permission of Elsevier Ltd.)

6.4.2 Dynamics of Polymeric Motion

The rate of chain and segmental motions is of the utmost importance, since these processes may determine the rate of the diffusional encounters and consequently the rate of the electron transport process within the polymer film. Below the glass transition temperature (T_m), the polymeric motion is practically frozen-in. Above T_m the frequency of the chain and segmental motions strongly increases with temperature [2, 202]. The plasticizing effect of the solvent enhances the rates of all kinds of motions in the polymer phase. At high electrolyte concentrations, the ionic shielding of the charged sites of the polymer increases, and the polymer film will adopt a more compact structure. In this case, the activity of the solvent is also low, and so the film swelling is less [2, 23, 200]. In the more compact structure, the molecular motions become more hindered. Covalent or electrostatic cross-linking diminishes the rates of all of the physical diffusion processes.

6.5 Effect of Film Structure and Morphology

In a general sense, the swollen polymer films can be considered to be polymer–polyelectrolyte gels. Various microscopic techniques have revealed a pronounced heterogeneity of the surface layer [2, 203–209]. In this respect, one must distinguish between macropores (the diameters of which considerably exceed 10 nm) and nanopores (which represent solvent molecules and ions between the polymer chains). Inside the macropores, the thermodynamic and transport properties of ions and solvent molecules are practically the same as those of the contacting bulk solution.

Space-charge regions (electric double layers) are formed at the interface between the polymer and solution phases, the thickness of which is much smaller than the characteristic sizes of macroelements (fibrils, grains, and pores). The polymer phase itself consists of a polymer matrix with incorporated ions and solvent molecules which do not form a separate continuous phase. Strong coulombic attractions between the electronic and ionic charges prevent them from being separated by a distance significantly exceeding the Debye screening length of the medium (ca. 0.1–0.3 nm in the charged state). There are three principal approaches to modeling the structure of the polymer phase [1, 193]. One may consider a uniform, homogeneous film [118, 190, 192–194], or a porous medium [31, 34, 86, 210–213], or an inhomogeneous homogeneous phase, where the properties of the first layer differ from those of the bulk film (see also Sect. 3.1.3). For uniform films, the polymer phase contains macromolecules, ions, and solvent molecules. In equilibrium its state is determined by the equality of the electrochemical potentials for all mobile species in all adjacent phases. Both electronic and ionic species participate in the formation of the space charges at the interfaces with the surrounding media, metal, and solution. The electroneutrality condition prevails inside the film; only a small imbalance from the charge related to the electric double layer species inside the metal or the solution parts of the interfaces is assumed. The overall electrode potential represents the sum of two interfacial contributions corresponding to the metal–polymer and polymer–solution interfaces. The potential distributions across the metal–film–solution depend on the electrolyte concentration and the partitioning equilibrium. At sufficiently high concentrations of co-ions inside the film, the potential drop at the polymer–solution interface is almost constant. In the opposite limiting case, the potential profile shows a gradual transformation as a function of charging level and the potential drops vary at both interfaces [118]. This model considers diffusion–migration transport of electronic and ionic charge carriers in a uniform medium, coupled with possibly nonequilibrium charge transfer across the corresponding interfaces at the boundaries of the film.

One extension of the uniform model is the inhomogeneous homogeneous model [136, 214], where due to the strong interactions between the adsorbed polymer molecules and the metal substrate (the nature of the metal and its surface geometry may play an important role), the properties of this layer are different from the rest

of the film. It can be described formally by introducing an adsorption pseudocapacitance and a resistance connected with the charging/discharging process within the first layer of the film at the metal interface.

The alternative approach, the porous medium model [31, 34, 107, 210–213, 215] separates polymer chains from ions and solvent molecules, placing them into two different phases. Physically, it represents a porous membrane which includes a matrix formed by the polymer and pores filled with electrolyte. Therefore, this macroscopically homogeneous two-phase system consists of an electronically conducting solid phase and an ionically conducting electrolyte phase. The transport properties of ions and solvent molecules in this phase may significantly differ from those in bulk electrolyte solutions. Each of these phases has specific electric resistivities (they may be inhomogeneous), and the two phases (i.e., their resistivities) are interconnected continuously by the double-layer capacitance at the surface between the solid phase and the pores. A further interconnection results from the charge transfer at the surface of the pores. There is also an electron exchange between the regions in the polymer with different degrees of oxidation. Despite seemingly opposite ways of describing the polymer phase in these approaches, the results concerning the responses to *dc* and *ac* perturbations often turned out to be similar or even identical.

Porosity effects during the charging process have long been considered in discussions of the faradaic and capacitive contributions to the current, especially in the case of electronically conducting polymers. For instance, the peaks of cyclic voltammograms were attributed to the faradaic process, while the plateaus of the current were considered to be an indication of the capacitive term [100, 106, 107, 216–220]. However, this straightforward analogy to the metal–solution interface does not work in reality; the obviously faradaic process of the redox transformation of the redox species in the surface layer does not lead to a direct current, unlike similar reactions for solute species.

6.5.1 Thickness

According to the theory of metastable adsorption of de Gennes [221], when an adsorbed polymer layer is in contact with a pure solvent, the layer density diminishes with increasing distance to the substrate (e.g., metal) surface. The behaviors of several polymer film electrodes, such as poly(tetracyanoquinodimethane) [135], poly(vinylferrocene) [150, 222], polypyrrole [223], and polyaniline [69, 224], have been explained by assuming that the local film density decreases with film thickness; that is, from the metal surface to the polymer–solution interface.

6.5.2 Synthesis Conditions and Nature of the Electrolyte

The film morphology (compactness, swelling) is strongly dependent on the composition of the solution, most notably on the type of counterions present in the solution used during electrodeposition and the plasticizing ability of the solvent molecules (see also Sect. 6.4). For instance, in the case of polyaniline BF_4^-, ClO_4^- and F_3CCOO^- promote the formation of a more compact structure, while the use of HSO_4^-, NO_3^-, or Cl^- results in a more open structure [109, 122, 204, 225]. Poly (vinylferrocene) is more swollen in the presence of SO_4^{2-} ions than in NO_3^- or ClO_4^--containing electrolytes. This means that the different anions enter the film together with their hydration spheres, since the magnitude of the mass change is as follows: sulfate > nitrate > perchlorate. This corresponds to the order of degree of hydration of these anions. On the other hand, the ion-pair formation constant for the oxidized sites and the ClO_4^- ions is greater than that for NO_3^- or SO_4^{2-} ions, which is reflected in the more positive formal potential of the ferrocene/ferricenium redox couple in Na_2SO_4 or $NaNO_3$ solutions compared with $NaClO_4$ electrolyte, as seen in Fig. 6.20.

The more pronounced swelling also reflects the more extensive interaction between water and the charged ferricenium sites in the presence of SO_4^{2-}- or NO_3^--compared to ClO_4^--containing electrolytes [121, 150]. Although in many papers it has been claimed that, once formed, the structure would be preserved even when the electrolyte used during electropolymerization is replaced by another one. However, this is not true. During cycling—albeit usually slowly—the morphology of the polymer layer changes, and eventually a structure characteristic of the polymer in that electrolyte develops. Figure 6.21 shows the results of such an experiment, when PANI film prepared in the presence of $HClO_4$ (see Fig. 4.2) was investigated in 5-sulfosalicylic acid (HSSA). In the presence of perchlorate ions, PANI adopts a more compact structure than in the solution of sulfosalicylic anions (SSA^-) (compare the respective Δf values in Fig. 4.2). However, slow ion exchange occurs during cycling as $HClO_4$ is replaced by HSSA. The original electroactivity is gradually regained, and the compact structure is simultaneously transformed into a less compact, more swollen one.

6.5.3 Effect of Electrolyte Concentration and Temperature

The swelling and shrinking of a polyelectrolyte gel are strongly affected by the concentration of the contacting electrolyte solution and the temperature [2, 19, 120, 121, 127]. Thermodynamic theory, which considers three contributions to the free energy of the gel (i.e., mixing of constituents, network deformation, and electrostatic interactions), predicts gel shrinkage as the salt concentration is increased or the temperature is decreased [226]. The shrinking process usually occurs smoothly, but under certain conditions the process becomes discontinuous, and the addition of

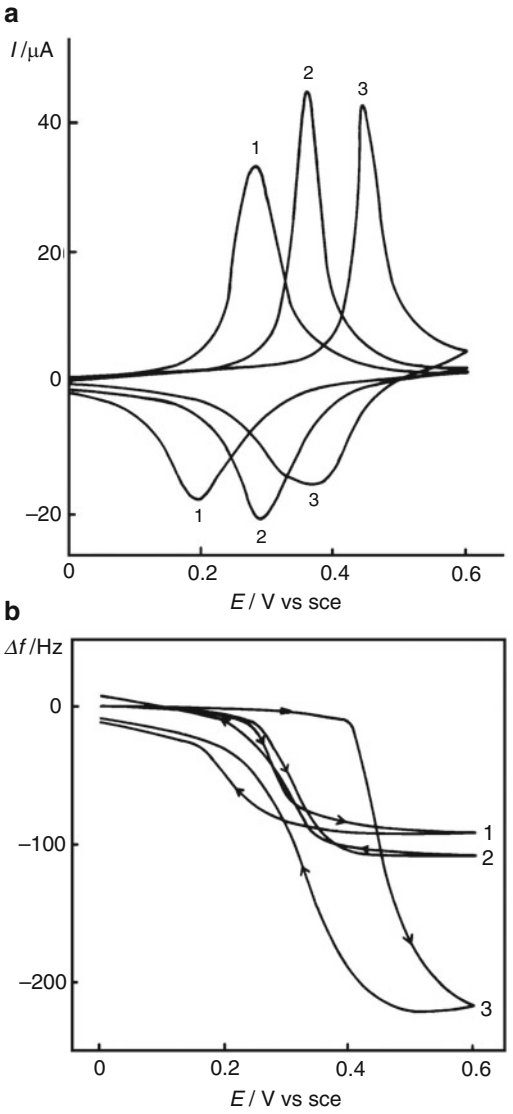

Fig. 6.20 Cyclic voltammograms (**a**) and the simultaneously recorded EQCN curves (**b**) for an electrochemically deposited PVF [poly(vinylferrocene)] film in contact with (*1*) $NaClO_4$; (*2*) $NaNO_3$; and (*3*) Na_2SO_4–H_2SO_4 pH 3.4, respectively. Electrolyte concentration: 0.5 mol dm^{-3}. Scan rate: 10 mV s^{-1} (Reproduced from [121] with the permission of Elsevier Ltd.)

a tiny amount of salt will lead to the collapse of the gel; i.e., a drastic decrease in the volume to a fraction of its original value.

The onset of shrinking and swelling substantially depends on temperature.

This phenomenon is akin to thermodynamic phase transitions in other branches of physical chemistry. The abrupt deterioration of the charge transport rate in poly (tetracyanoquinodimethane); Fig. 6.22 or poly(vinylferrocene) films [23] at high electrolyte concentrations (10 mol dm^{-3} LiCl or 5 mol dm^{-3} $CaCl_2$) and its temperature dependence (Fig. 6.23) can be interpreted based on thermodynamic

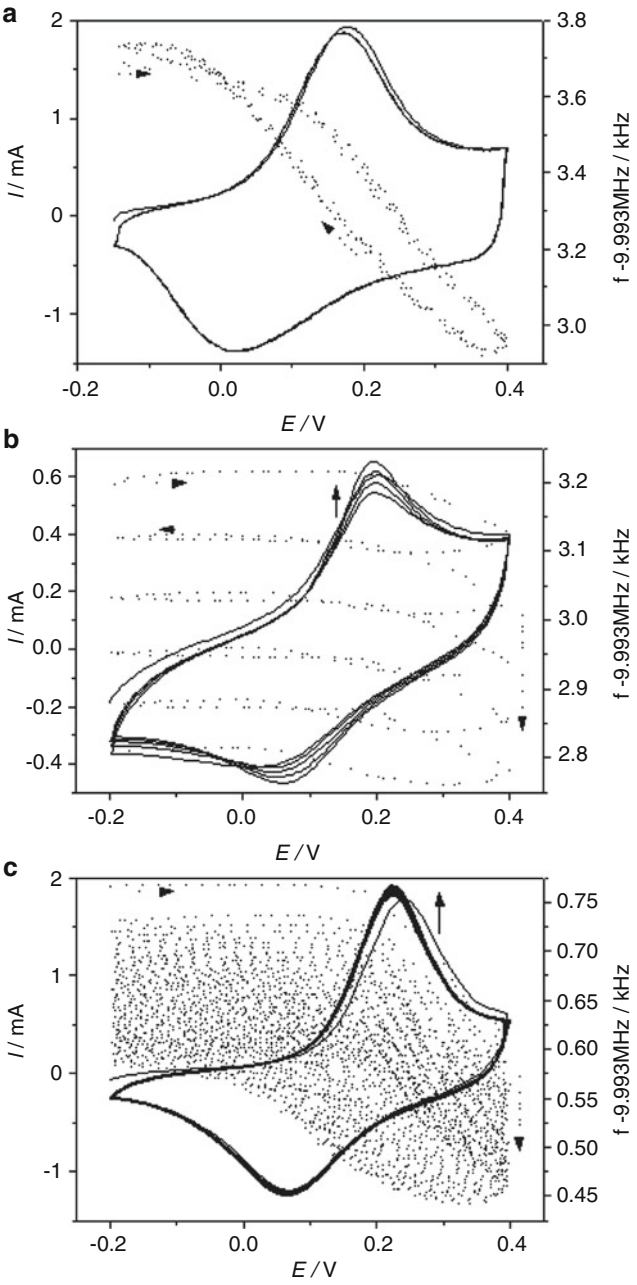

Fig. 6.21 Cyclic voltammograms and the simultaneously obtained EQCN frequency curves recorded for a PANI electrode (**a**) in 1 mol dm^{-3} $HClO_4$ (**b**) and (**c**) in 1 mol dm^{-3} 5-sulfosalicylic acid (HSSA) after exchanging $HClO_4$ for HSSA. The *curves* shown in (**b**) were taken during the first five cycles after the solution had been replaced, while those in (**c**) display the current and frequency responses from the 135th to the 175th cycles. Scan rate: 100 mV s^{-1} (Reproduced from [122] with the permission of Elsevier Ltd.)

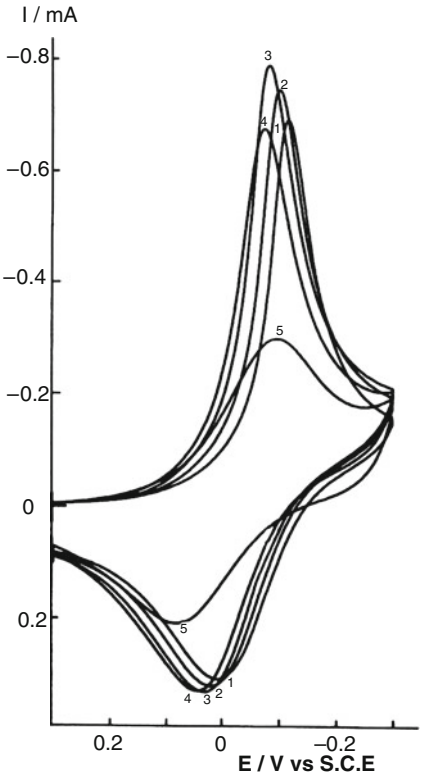

Fig. 6.22 Cyclic voltammograms of a poly (tetracyanoquinodimethane) electrode (Γ =13 nmol cm^{-2}) in contact with lithium chloride solution at different concentrations: (*1*) 0.625, (*2*) 1.25, (*3*) 2.5, (*4*) 5.0, and (*5*) 10.0 mol dm^{-3}. Sweep rate: 60 mV s^{-1} (Reproduced from [20] with the permission of Elsevier Ltd.)

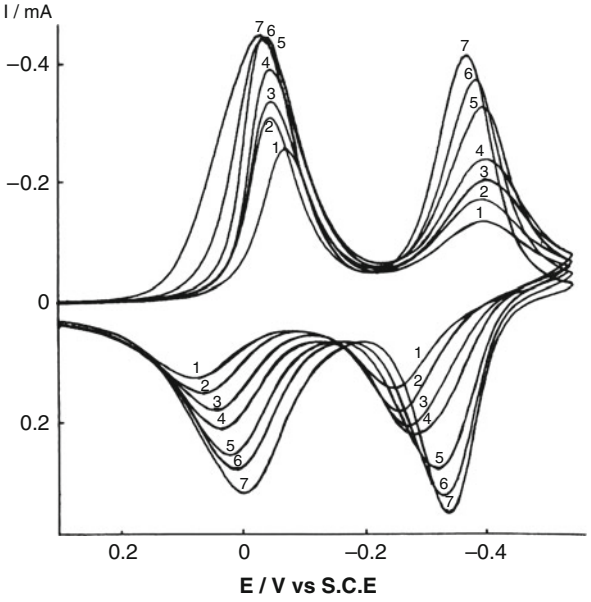

Fig. 6.23 Cyclic voltammograms of a PTCNQ electrode ($\Gamma = 5.1 \times 10^{-8}$ mol cm^{-2}) in contact with aqueous 10 M LiCl. Scan rate: 6 mV s^{-1}. Temperature: (*1*) 22, (*2*) 34, (*3*) 44, (*4*) 50, (*5*) 61, (*6*) 66, and (*7*) 77°C (Reproduced from [227] with the permission of Elsevier Ltd.)

theory [20, 23, 227]. In a more compact structure, the rate of electron hopping may increase since the concentration of redox (c) sites is high; however, a deterioration in the film's permeability to the counterions due to the decrease in the free volume is expected at the same time. The maximum observed in the peak current versus salt concentration curve is the result of the balanced effects of the enhanced electron exchange process and the hindered counterion motion. The abrupt change in the free volume of solvent-filled cavities causes a sharp decrease in the charge transport diffusion coefficient [2, 20, 23, 227, 228]. A rigorous theoretical treatment which takes into account the extension and contraction of the polymer chain as it is electrochemically converted into a polyelectrolyte is very difficult if not impossible due to the complexity of the polyelectrolyte systems and the lack of an appropriate set of data. Inzelt et al. [2, 20] modeled these effects in an empirical approach by scaling the concentration of electroactive sites in the polymer film and the effective charge transport diffusion coefficient (D_{ct}) with $c_s^{1/2}$.

By employing the empirical equations

$$c = Z(1 + Bc_s^{1/2}), \tag{6.29}$$

and

$$D = D^o(1 - H'c). \tag{6.30}$$

A semiquantitative description of the effect of concentration on peak currents and peak potentials has been obtained. D_{ct}^o is the effective diffusion coefficient of charge transport through the polymer film in the absence of the addition of supporting electrolyte; Z, B, and H' are empirical parameters characteristic of the system under study. The values of these parameters depend on the nature of the solvent, the counterions (their size and charge), and the polymer forming the film. Combining (6.29) and (6.30) with the Randles–Ševčík equation, as well as the appropriate Nernst equation, gives the relationship

$$I_p = K_i[1 - H(1 + Bc_s^{1/2})]^{1/2}(1 + Bc_s^{1/2}), \tag{6.31}$$

and

$$E_p = K_E + \frac{RT}{zF} \ln\{c_s[1 - H(1 + Bc_s^{1/2})]^{1/2}\}, \tag{6.32}$$

where

$$K_i = 2.69 \times 10^5 D_{ct}^{\circ 1/2} A v^{1/2} Z \quad \text{and } H = ZH',$$

$$K_E = E_c^{\Theta'} - \frac{RT}{zF} \ln K \pm 0.0285.$$

The constant in the equation of the peak current (K_i) includes the quantities in the Randles–Ševčík equation; i.e., A is the electrode area, v is the scan rate, and the charge number of the electrode reaction is assumed to be 1. The constant in the equation of the peak potential (K_E) contains the formal potential ($E_c^{\ominus\prime}$) and the formation constant of the salt, ion pair, or complex (K). +0.0285 V and −0.0285 V, respectively, have to be used for the anodic and cathodic peak potentials. The + or a− sign that appears before the term of (RT/zF) ln K depends on the type of ions exchanged. When counterions enter the polymer film, the sign is + for reduction and − for oxidation, respectively. For instance, for the reduction of TCNQ [see (2.1)], the sign is positive. However, when co-ions leave the film, the opposite sign applies, i.e., during oxidation [see (6.26) and (6.27)] the sign is positive. The most remarkable conclusion of these calculations is the fact that the variation in the I_p and E_p values with c_s can be described with the same set of parameters for a given system. In addition, the variation in Z, which is characteristic of the chemical structure of the film, B, which in turn is linked to the swelling (solvent–polymer and ion–polymer interactions) and H, which expresses how the permeability of the film depends on the sizes of the penetrating ions and the solvent-filled cavities (the free volume in the film), exhibited rather reasonable, systematic changes as the solvent was replaced with a better one or univalent ions were substituted for bivalent ones.

6.6 Relaxation and Hysteresis Phenomena

Owing to the long relaxation times characteristic of polymeric systems, the equilibrium or steady-state situation is often not reached within the time scale of the experiment. Figure 6.24 shows the change in the resistance of polyaniline after potential steps.

It can be seen that the achievement of a constant resistance value takes a rather long time, especially during the conducting-to-insulating transition. Consequently, even slow sweep rate cyclic voltammetry does not supply reliable thermodynamic quantities that can otherwise be derived by analyzing the changes in the peak potentials. The polymeric nature of these systems is most strikingly manifested in the relaxation phenomena linked to changes in the conditions (potential, temperature, etc.) which appear in different effects such as the hysteresis, "first cycle," and memory effects [19, 54, 89, 109, 111, 147, 219, 228–239].

The first cycle or waiting time effects (where the shapes of the cyclic voltammograms and the peak potentials depend on the delay time at potentials at which the polymer is in its neutral/discharged state: see also "secondary break-in") have been interpreted in terms of slow morphological changes and/or the difficulty removing the remaining charges from insulating surroundings [228, 230, 231]. It should be mentioned that this problem also arises in the case of redox polymers [19, 23, 130–132]. The results of fast scan rate voltammetry, chronoamperometry, and chronopotentiometry have also been explained by a model assuming instantaneous two-dimensional nucleation and growth of conducting zones, and it was concluded that oxidation and reduction must proceed by different pathways and involve different

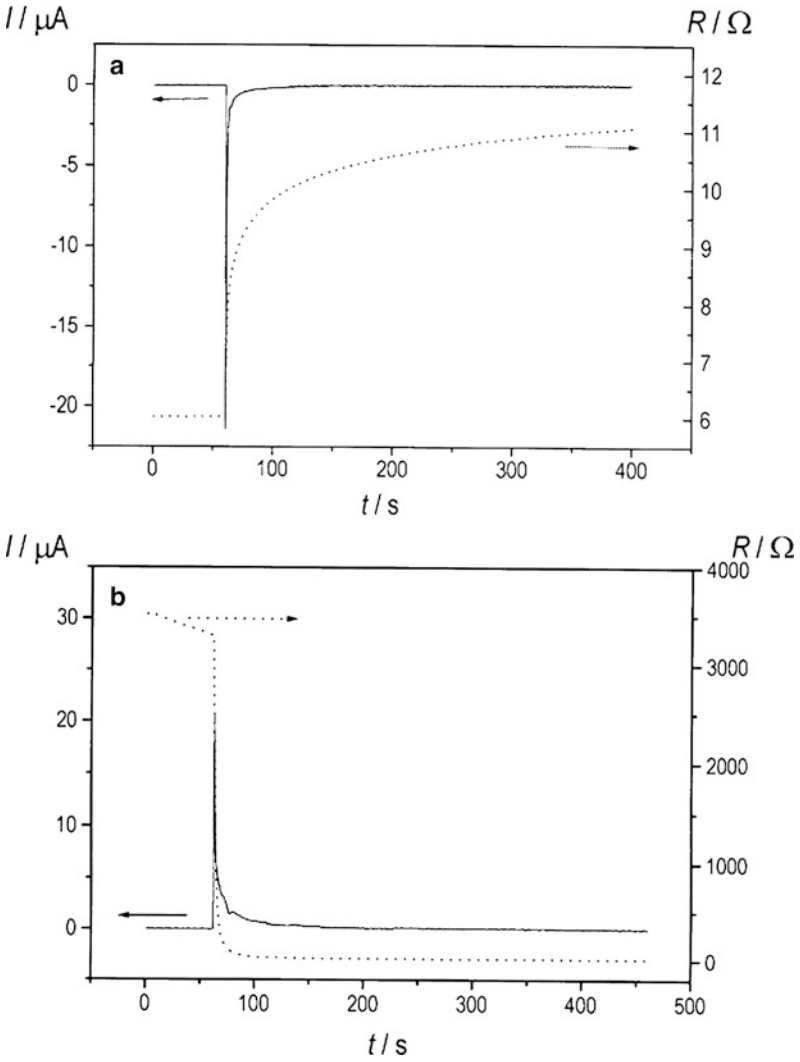

Fig. 6.24 The current transients and the respective resistance–time curves obtained after performing potential steps (**a**) from 0.2 to 0.15 V and (**b**) from 0.15 to 0.2 V for a PANI electrode in contact with 2 mol dm^{-3} H_2SO_4 (Reproduced from [54] with the permission of Elsevier Ltd.)

degrees of disorder [109, 240]. The slow change in the local pH has also been accounted for [229]. For the conducting-to-insulating conversion, the slow relaxation effect has been interpreted within the framework of percolation theory [236, 241] and by the electrochemically stimulated conformational relaxation (ESCR) model [111, 174, 242, 243]. Both of these theories predict a logarithmic time dependence. The percolation theory assumes that the slow relaxation after rapid conducting–insulating conversion is composed of three interrelated processes: statistical structure formation,

random fluctuations, and electron transfer. Accordingly, the rate-determining step is either the electrochemical reaction that occurs in electrode-percolated conducting clusters or the random rearrangement of conducting clusters by electron exchange reactions between the conducting and insulating species and/or the diffusion of polymer chains. The rate of the conducting–insulating conversion suddenly slows down at the percolation threshold.

In the percolation models elaborated by Aoki and coworkers [234–236, 241, 244–246], it is assumed that the C ("conducting") species produced by the electrochemical oxidation act as a metal-like electrode in converting the I ("insulating") species into the C species. The C domain generates itself, growing toward the solution phase with a well-defined boundary between the C and the I zones. The rate of oxidation is controlled by the rate of electron transfer from the C zone to the I zone; in a first approach the influence of the ionic charge transport is neglected. Electric double layers may form not only at the boundary between the two zones but also at the microscopic interfaces between C species and the solution penetrating into the C domain. Since the double layer is distributed over the film in the C state, the reduction is allowed to occur at any position or preferentially at the most active sites in the C domain. During reduction, a random conversion takes place in the C microdomains, which have electric connections with the metal substrate. The conversion proceeds until the molar fraction of the C species decreases to a threshold of percolation. As a result, some of the C species is left behind in the film, forming a fractal geometry [234]. The C species remaining in the film can be transported to the electrode by diffusion, or their reduction may occur via electron hopping. Since only a small proportion of the C zones are connected electrically to the metal below the percolation threshold, the conversion rate becomes very slow. This manifests itself in the slow relaxation, which is characterized by the variations in the polymer film over times of as long as a few hours. This is the main cause of the phenomena known as the memory effect, the first cycle effect, and hysteresis. The key parameter of slow relaxation is the electrolysis time in the I state, often called a waiting time, t_w. The anodic peak potential, peak current, and the spin concentration depend logarithmically on t_w. Aoki investigated the dependence of the faradaic charge associated with the switching of PANI films [244].

A distribution of C clusters was assumed. Some clusters are in contact with the metal, while others are surrounded by other C species and I species. The rate-determining step is the charge transfer rate at the C–I interface or the formation of C clusters. For the time (t) dependence of the charge consumed (q), the following equation was derived:

$$q = q_T(1-p) = q_T + \frac{q_T}{a}\ln\left[\left(\frac{aks_o}{q_T}\right)t + \exp(-ap_c)\right], \tag{6.33}$$

where q_T is the total charge associated with the redox reaction; p is related to the ratio of the concentrations of the oxidized (c_o) and reduced (c_R) species [i.e., $p = c_o/(c_o + c_R)$; a is the probability of creating C clusters for small variations in p]; k is the

rate coefficient per volume of the reduction ($q_T dp/dt = -ks$), a potential-dependent quantity; s is the volume of all percolated clusters; s_o is the volume of the percolation threshold (p_c). Since $0 \leq p \leq 1$ or $0 \leq q \leq q_T$, (6.29) has a maximum of t.

It was derived [244] that $p_c = 0.23$, and so the term $\exp(-ap_c)$ is negligibly small. Therefore, the equation for the logarithmic dependence of q on the waiting time t_w is

$$q = q_T \left[\left(\frac{1}{a} \right) \ln t_w + \left(\frac{1}{a} \right) \ln \left(\frac{aks_o}{q_T} \right) + 1 \right] \tag{6.34}$$

The value of a was determined from the q vs. ln t_w plots; and it was found that a is not constant but is instead proportional to ${q_T}^{-0.29}$. Consequently, the volume increase as a function of p can be obtained from the following equation:

$$s = p_c \exp\left[a' {q_T}^{-0.29} (p - p_c) \right], \tag{6.35}$$

where a' is a constant. The relaxation behavior of PANI has been analyzed in several papers using percolation theory [234–236, 241, 244–246].

The ESCR model assumes that two main processes are operative concerning the kinetics of the redox switching of conducting polymers. First is the charging–-discharging process, which includes electronic and ionic charge transport. Second is the induced conformational change in the polymer that affects the rate of the electrochemical transformation, and due to the slowness of the relaxation of the polymer this process may last much longer than the actual oxidation or reduction process. The latter model was used to describe the redox switching of polypyrrole, where an extensive volume increase occurs during oxidation. It should be taken into account that extramechanical energy is needed to open the originally compact structure. The hysteresis effect has been explained by the difference in the oxidation and reduction sequences.

According to the ESCR model, the following steps should be considered. Upon applying an anodic overpotential to a neutral conjugated polymer, an expansion of the closed polymeric structure occurs initially. In this way, partial oxidation takes place and under the influence of an electrical field counterions from the solution enter the solid polymer at those points in the polymer/electrolyte interface where the structure is less compact. This is called the nucleation process. Then the oxidized sphere expands from these points toward the polymer/metal interface and grows parallel to the metal surface. The rate of this part of the overall reaction is controlled by a structural relaxation involving conformational changes of polymer segments and a swelling of the polymer due to electrostatic repulsions between the chains and incorporations of counterions (see Fig. 6.25). The oxidation process is completed by the diffusion of counterions through the previously opened structure of the polymer. Opposite processes occur during reduction. The positive charges on the polymers are neutralized and counterions are expelled. Reverse conformational changes lead to a shrinking of the polymer. Diffusion of the

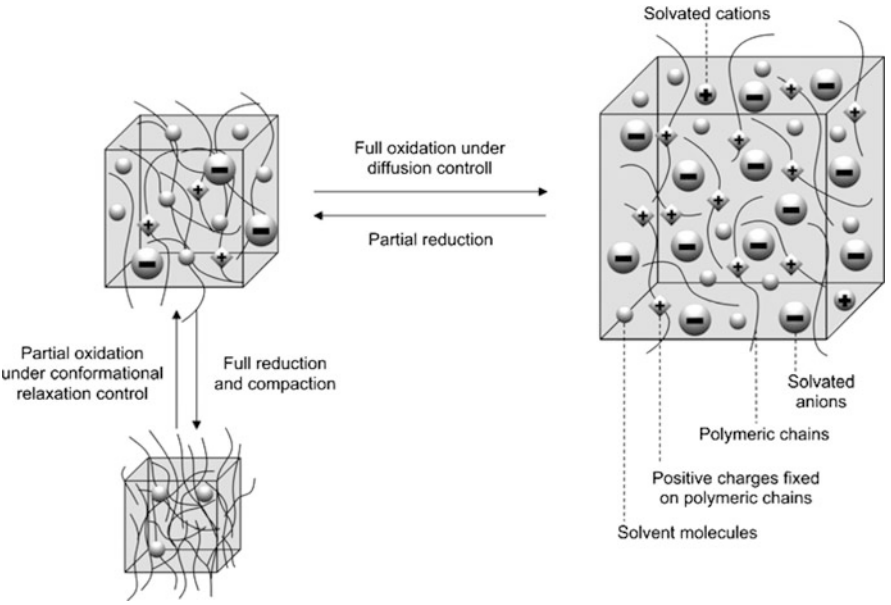

Fig. 6.25 Illustration of the ESCR model (Reproduced from [174] with the permission of Elsevier Ltd.)

counterions becomes more and more difficult. The structure is closing. The degree of compaction that takes place during this closing step depends on the cathodic potential applied to the polymer and will be more efficient at more negative potentials. The compact structure hinders counterion exchange with the solution. A quantitative expression for the relaxation time τ needed to open the closed polymer structure is as follows:

$$\tau = \tau_o \exp[\Delta H^* + z_c(E_s - E_c) - z_r(E - E_o)], \tag{6.36}$$

where ΔH^* is the conformational energy consumed per mole of polymeric segments in the absence of any external electrical field; the second term $z_c(E_s - E_c)$ is the energy required to reduce, close, and compact one mole of polymeric segments, with E_s = experimental potential of closure and E_c = compaction potential, and finally $z_r(E - E_o)$ represents the energy required to open the closed structure. (z_r = charge consumed to relax one mol of polymeric segments; τ_o = relaxation time in the absence of any polarization effects.)

The hysteresis effect and the non-Nernstian behavior for polyaniline have also been elucidated with the help of polaron models by considering that the formation energies of both polarons and bipolarons increase as the degree of oxidation increases [86, 212]. A first-order phase transition due to an S-shaped energy diagram that is in connection with attractive interactions between electronic and ionic charges has also been proposed [239]. The hysteresis phenomenon has also been explained by the stabilization of the oxidized polymer molecules by

considering that the originally twisted, benzoid conformation is transformed into a more planar, quinoid-like structure with better π-conjugation, which can therefore be reduced at lower potentials (with lower energy). The planarization of the twisted segments within a chain takes place during the first stage of the charging process, and due to the interactions between the π-electron clouds of the neighboring charged segments intermolecular stabilization can also occur. Intermolecular interactions are favorable in the crystalline domains of the polymer. It is assumed that the stabilization process is fast [100]. Even an intermolecular coupling of the two π-radical centers forming a σ-bond and the dimerization and disproportion of polaronic segments have also recently been proposed [71, 113, 114]. Vorotyntsev and Heinze [114] elaborated a concept based on two coexisting subsystems in the polymer matrix, i.e., the usual neutral, cation radical (polaron), and dication (bipolaron) sites, and entities representing a couple of sites where intermolecular bonds between neighboring molecules are formed. These bonds may be either π-bonds or σ-bonds, and the dimers may also exist in neutral, charged, and doubly charged states. The idea was based on the results obtained when charging and discharging PPP films, which indicated that there are reversible or quasi-reversible and irreversible processes depending on the potential intervals investigated for the oxidation and reduction processes, respectively. In this work, the distribution of redox potentials (energetic inhomogeneity) was also considered. The concentration distributions of the various species were calculated by using reasonable assumptions for the values of different equilibrium and kinetic quantities. One of the results of these calculations, where the dispersion of the redox potentials of the undimerized forms has also been taken into account, is shown in Fig. 6.26.

During the anodic scan, the neutral form (D_{00}) initially transformed into a singly charged form (D_{01}). This was then gradually replaced by the σ-bond state (D_σ). The concentrations of D_{11} and D_π are also noticeable within this potential interval.

During reduction, the concentration profiles are quite different; the radical form (D_r) appears in substantial amounts as an intermediate. Because the potential range in which the given species exists is shifted, a hysteresis can be observed in the potential variations in the principal concentrations of species D_{00} and D_σ. The corresponding theoretical cyclic voltammograms are presented in Fig. 6.27. Paasch analyzed the hysteresis in terms of dissociation of bipolarons [89].

It is worth mentioning that the considerable difference between the anodic and cathodic peak potentials of the cyclic voltammograms for the poly(tetracyanoquinodimethane) redox electrode (Fig. 6.22) has been explained by the formation of dimeric species; i.e., the slow formation of mixed-valence dimers during reduction (charging) and the fast reoxidation of dimer dianions resulting in mixed-valence dimers during the discharging process [19, 127].

The concentrations of the anion radicals and the dimer dianions were derived from UV–VIS spectroelectrochemical data. The concentration of the mixed-valence dimer was calculated from the variation in the ESR intensity and the concentration of the other paramagnetic species, $TCNQ^{\bar{\bullet}}$ [127] (see Fig. 6.28).

The shielding effects of the counterions may also contribute to the overall stabilization energy.

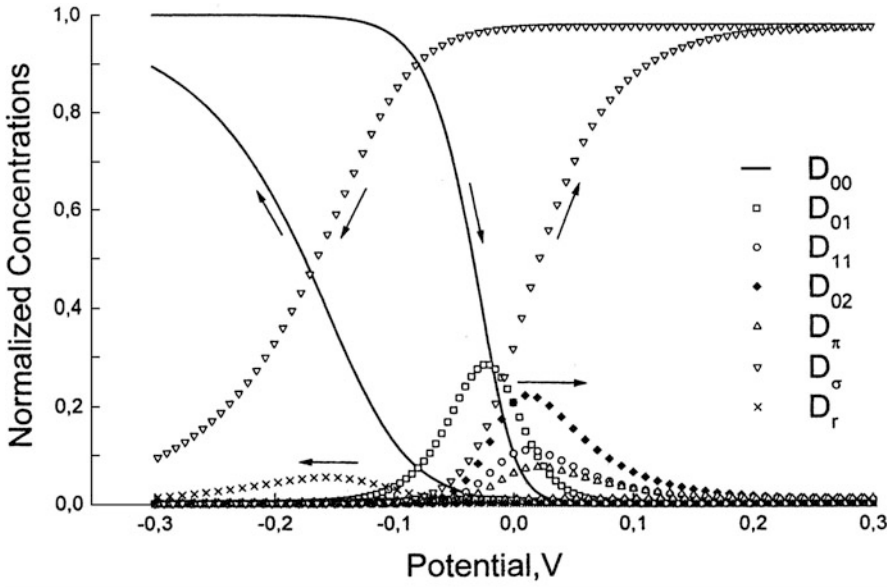

Fig. 6.26 Variations in the concentrations of various dimerized forms during cyclic voltammetry. A broad energy distribution was considered for the undimerized sites, whereas each dimerized state (D) was characterized by a single redox potential. D_{00}, D_{01}, D_{02}, D_{11}, D_{π}, D_{σ}, and D_{r} symbolize the different dimers, where the indices 0, 1, and 2 indicate neutral, singly, and doubly charged species, respectively; e.g., D_{01} is a dimer of a neutral and a singly charge entity. D_{π} is a π-bond complex between the neighboring molecules, and D_{σ} is a corresponding σ-bond complex, while D_{r} is a partially discharged σ-bond complex (Reproduced from [114] with the permission of Elsevier Ltd.)

The hysteresis phenomenon was analyzed in terms of two classes: dynamic hysteresis containing a kinetic and an ohmic component, and stationary or thermodynamic hysteresis. It was concluded that the hysteresis in cyclic voltammograms observed for poly(3-methylthiophene) is mainly kinetic in nature, while for PANI the hysteresis (which is independent of scan rate and current) has a thermodynamic origin [230].

While the effect of potential-induced relaxation phenomena has been studied extensively, less effort has been expended in exploring the effect of temperature. One notable exception is a temperature shock experiment on a poly(tetracyanoquinodimethane) electrode. It was found that when the electrode returned from elevated temperature to room temperature, a relatively long time (>30 min) was needed to restore the original room temperature voltammetric response, as seen in Fig. 6.29.

Apparently, the polymer adopts an extended, perhaps solvent-swollen conformation at elevated temperatures that requires a long time to revert back to the room temperature structure [19, 227]. Such behavior is observed in studies of polymer gels, where varying the temperature results in the hysteresis of macroscopic polymer properties such as swelling, elasticity, and turbidity.

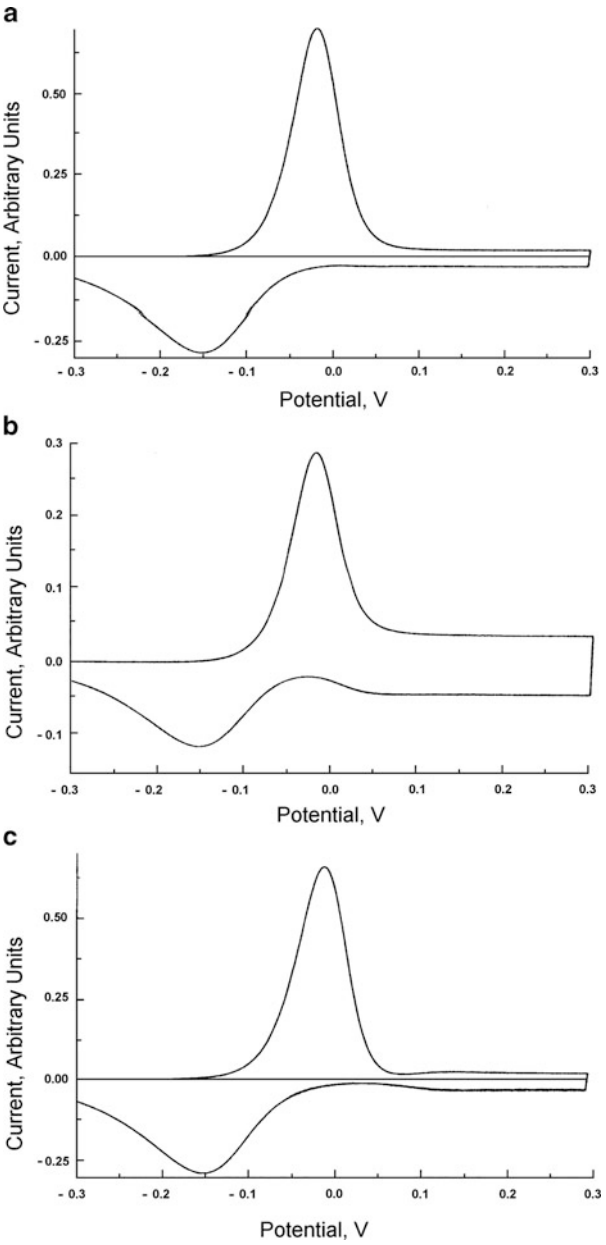

Fig. 6.27 The cyclic voltammograms predicted by the dimerization model with energetic inhomogeneity of undimerized sites. *Curves* (**a**)–(**c**) were simulated by using different fractions of thedimerized forms, and for (**a**) and (**b**) $E^{\Theta\prime}_{c,2} - E^{\Theta\prime}_{c,1} = 0$, while for (**c**) $E^{\Theta\prime}_{c,2} - E^{\Theta\prime}_{c,1} = 0.1\,\mathrm{V}$, where $E^{\Theta\prime}_{c,2}$ and $E^{\Theta\prime}_{c,1}$ represent the formal potentials of the two redox reactions (Reproduced from [114] with the permission of Elsevier Ltd.)

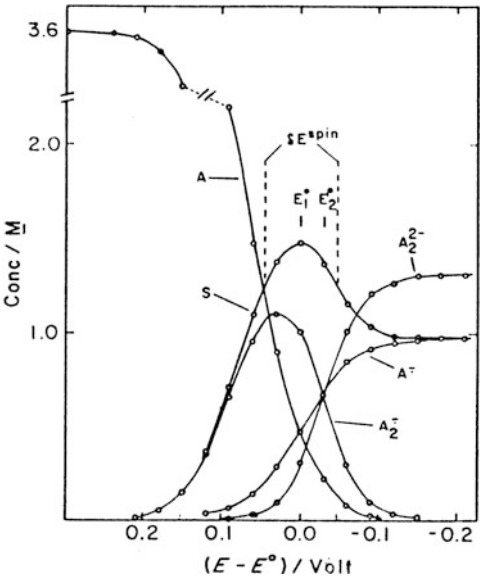

Fig. 6.28 Distribution diagram for the species formed during the electroreduction of poly (tetracyanoquinodimethane). A = TCNQ, $A^{-\bullet} = TCNQ^{-\bullet}$, $A_2^{\bullet-} = TCNQ_2^{\bullet-}$, $A_2^{2-} = TCNQ_2^{2-}$, and $S = c_{TCNQ^{-\bullet}} + c_{TCNQ_2^{\bullet-}}$ [127]

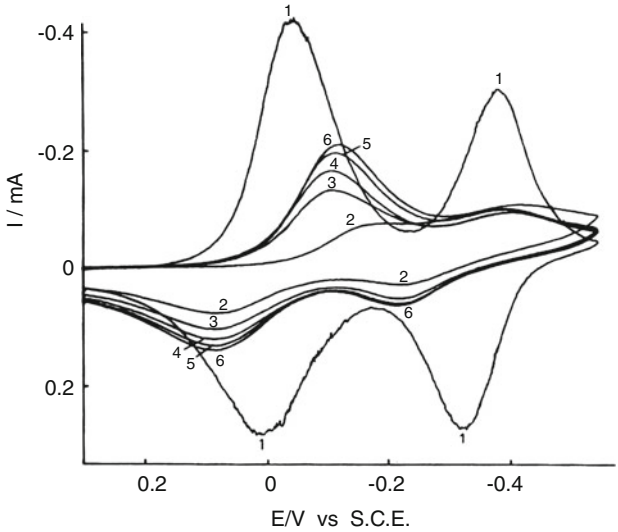

Fig. 6.29 Cyclic voltammograms obtained for a poly(tetracyanoquinodimethane) electrode in contact with 10 M LiCl at (*1*) 69°C and (*2–6*) after rapid cooling at 22°C, recorded after delays of (*2*) 4, (*3*) 9, (*4*) 13.5, (*5*) 22.5, and (*6*) 38.5 min (Reproduced from [227] with the permission of Elsevier Ltd.)

6.7 Measurements of the Rate of Charge Transport

The rate of charge transport within an electrochemically active polymer film has been successfully studied by transient electrochemical techniques. One may distinguish between methods using large and small potentials or current perturbations. Cyclic voltammetry and potential (less often current) step and pulse techniques have been applied for basic characterization. Average values for the charge transport diffusion coefficient can be obtained using these techniques, since the properties of the polymer change continuously and large amounts of ions and/or solvent molecules are exchanged between the polymer phase and the bulk solution during the experiments. Owing to the marginal perturbations from equilibrium (steady state) caused by low-amplitude (<5 mV) sinusoidal voltage, electrochemical impedance spectroscopy (EIS) is evidently advantageous compared to other techniques involving large perturbations. The actual reaction mechanism may be elucidated and the rate-determining step assigned using combined techniques. Information on these techniques and references associated with them can be found in Chap. 3.

References

1. Inzelt G, Pineri M, Schultze JW, Vorotyntsev MA (2000) Electrochim Acta 45:2403
2. Inzelt G (1994) Mechanism of charge transport in polymer-modified electrodes. In: Bard AJ (ed) Electroanalytical chemistry, vol 18. Dekker, New York, p 89
3. Lyons MEG (ed) (1994) Electroactive polymer electrochemistry, part I. Plenum, New York
4. Lyons MEG (ed) (1996) Electroactive polymer electrochemistry, part II. Plenum, New York
5. Malev VV, Kontratiev VV (2006) Russ Chem Rev 75:147
6. Murray RW (1984) Chemically modified electrodes. In: Bard AJ (ed) Electroanalytical chemistry, vol 13. Dekker, New York, p 191
7. Murray RW (ed) (1992) Molecular design of electrode surfaces. In: Weissberger A, Saunders H Jr (eds) Techniques of chemistry, vol 22. Wiley, New York
8. Vorotyntsev MA, Levi MD (1991) Elektronno–provodyashchiye polimeri. In: Polukarov YuM (ed) Itogi nauki i tekhniki, vol 34. Viniti, Moscow
9. Dahms H (1968) J Phys Chem 72:362
10. Ruff I, Friedrich VJ (1971) J Phys Chem 75:3297
11. Ruff I, Friedrich VJ, Demeter K, Csillag K (1971) J Phys Chem 75:3303
12. Botár L, Ruff I (1986) Chem Phys Lett 126:348
13. Buck RP (1988) J Phys Chem 92:4196
14. Buck RP (1987) J Electroanal Chem 219:23
15. Buck RP (1988) J Phys Chem 92:6445
16. Buck RP (1989) J Electroanal Chem 258:1
17. Rubinstein I (1985) J Electroanal Chem 188:227
18. Albery WJ, Hillman AR (1981) Ann Rev C R Soc Chem Lond 377
19. Inzelt G (1989) Electrochim Acta 34:83
20. Inzelt G, Chambers JQ, Bácskai J, Day RW (1986) J Electroanal Chem 201:301
21. Schroeder AH, Kaufman FB (1980) J Electroanal Chem 113:209
22. Hillman AR, Loveday DC, Swann MJ, Eales RM, Hamnett A, Higgins SJ, Bruckenstein S, Wilde CP (1989) Faraday Disc Chem Soc 88:151

23. Inzelt G, Szabó L (1986) Electrochim Acta 31:1381
24. Dalton EF, Murray RW (1991) J Phys Chem 95:6383
25. Buttry DA, Anson FC (1981) J Electroanal Chem 130:333
26. Feldberg SW (1986) J Electroanal Chem 198:1
27. Láng G, Inzelt G (1991) Electrochim Acta 36:847
28. Gabrielli C, Takenouti H, Haas O, Tsukada A (1991) J Electroanal Chem 302:59
29. Oyama N, Yamaguchi S, Nishiki Y, Tokuda K, Anson FC (1982) J Electroanal Chem 139:371
30. Rubinstein I, Risphon J, Gottesfeld S (1986) J Electrochem Soc 133:729
31. Penner R, Martin CR (1989) J Phys Chem 93:984
32. Hunter TB, Tyler PS, Smyrl WH, White HS (1987) J Electrochem Soc 134:2198
33. Nakahama S, Murray RW (1983) J Electroanal Chem 158:303
34. Paulse CD, Pickup PG (1988) J Phys Chem 92:7002
35. He P, Chen X (1988) J Electroanal Chem 256:353
36. Fritsch-Faules I, Faulkner LR (1989) J Electroanal Chem 263:237
37. Blauch DN, Savéant JM (1992) J Am Chem Soc 114:3323
38. Leiva E, Meyer P, Schmickler W (1988) J Electrochem Soc 135:1993
39. Chidsey CED, Murray RW (1986) J Phys Chem 90:1479
40. Andrieux CP, Saveant JM (1980) J Electroanal Chem 111:377
41. Andrieux CP, Saveant JM (1988) J Phys Chem 92:6761
42. Saveant JM (1988) J Electroanal Chem 242:1
43. Saveant JM (1988) J Phys Chem 92:4526
44. Baldy CJ, Elliot CM, Feldberg SW (1990) J Electroanal Chem 283:53
45. Laviron E (1980) J Electroanal Chem 112:1
46. Srinivasa Mohan L, Sangaranarayanan MV (1992) J Electroanal Chem 323: 375
47. MacDiarmid AG (2001) Angew Chem Int Ed 40:2581
48. Heeger AJ (2001) Angew Chem Int Ed 40:2591
49. Diaz AF, Rubinson JF, Mark HB Jr (1988) Electrochemistry and electrode applications of electroactive/conducting polymers. In: Henrici-Olivé G, Olivé S (eds) Advances in polymer science, vol 84. Springer, Berlin, p 113
50. Evans GP (1990) The electrochemistry of conducting polymers. In: Gerischer H, Tobias CW (eds) Advances in electrochemical science and engineering, vol 1. VCH, Weinheim, p 1
51. Skotheim TA (ed) (1998) Handbook of conducting polymers. Dekker, New York
52. Genies EM, Boyle A, Lapkowski M, Tsintavis C (1990) Synth Met 36:139
53. Asturias GE, Jang GW, MacDiarmid AG, Doblhofer K, Zhong C (1991) Ber Bunsenges Phys Chem 95:1381
54. Csahók E, Vieil E, Inzelt G (2000) J Electroanal Chem 482:168
55. Epstein AJ, MacDiarmid AG (1991) Synth Met 41–43:601
56. Focke WW, Wnek GE, Wei Y (1987) J Phys Chem 91:5813
57. Glarum SH, Marshall JH (1987) J Electrochem Soc 134:142
58. Zhang C, Yao B, Huang J, Zhou X (1997) J Electroanal Chem 440:35
59. Romero AJF, Cascales JJL, Otero TF (2005) J Phys Chem B 109:21078
60. Miasik J, Hooper A, Tofield B (1986) J Chem Soc Faraday Trans 82:1117
61. Syritski V, Öpik A, Forsén O (2003) Electrochim Acta 48:1409
62. Naarmann H (1987) Synth Met 17:223
63. Swager TM (1998) Acc Chem Res 31:201
64. Conwell EM (1997) In: Nalwa HS (ed) Handbook of organic conducting molecules and polymers, vol 4. Wiley, New York, p 1
65. Tsukamoto J, Takahashi A, Kawasaki K (1990) Jap J Appl Phys 29:125
66. Csahók E, Vieil E, Inzelt G (1999) Synth Met 101:843
67. Wessling B (1994) Adv Mater 6:226
68. Norris ID, Shaker MM, Ko FK, MacDiarmid AG (2000) Synth Met 114:109
69. Glarum SH, Marshall JH (1987) J Electrochem Soc 134:2160
70. Mazeikiene R, Niaura G, Malinauskas A (2006) Electrochim Acta 51:1917

71. Neudeck A, Petr A, Dunsch L (1999) J Phys Chem B 103:912
72. Petr A, Dunsch L (1996) J Electroanal Chem 419:55
73. Zhou Q, Zhuang L, Lu J (2002) Electrochem Commun 4:733
74. Zhuang L, Zhou Q, Lu J (2000) J Electroanal Chem 493:135
75. Albery WJ, Chen Z, Horrocks BR, Mount AR, Wilson PJ, Bloor D, Monkman AT, Elliot CM (1989) Faraday Disc Chem Soc 88:247
76. Scott J, Pfluger P, Krounbi MT, Street GB (1983) Phys Rev B 28:2140
77. Neudeck A, Marken F, Compton RG (2002) UV/VIS/NIR spectroelectrochemistry. In: Scholz F (ed) Electroanalytical methods. Springer, Berlin, pp 167–189
78. Patil R, Harima Y, Yamashita K, Komaguchi K, Itagaki Y, Shiotani M (2002) J Electroanal Chem 518:13
79. MacDiarmid AG, Epstein AJ (1989) Faraday Disc Chem Soc 88:317
80. Kaufman JH, Kanazawa KK, Street JB (1984) Phys Rev Lett 53:2461
81. Skotheim TA (ed) (1986) Handbook of conducting polymers. Dekker, New York, vols 1–2
82. Chance RP, Boudreaux DS, Bredas JL, Silbey R (1986) In: Skotheim TA (ed) Handbook of conducting polymers, vol 2. Dekker, New York, p 825
83. Heeger AJ (1989) Faraday Disc Chem Soc 88:203
84. Bredas JL, Street GB (1985) Acc Chem Res 18:309
85. Paasch G (1992) Synth Met 51:7
86. Paasch G, Nguyen PH, Fischer AJ (1998) Chem Phys 227:219
87. Vorotyntsev MA, Daikhin LI, Levi MD (1992) J Electroanal Chem 332:213
88. Vorotyntsev MA, Rubashkin AA, Badiali JP (1996) Electrochim Acta 41:2313
89. Paasch G (2007) J Electroanal Chem 600:131
90. Mott NF, Davis EA (1979) Electronic processes in non-crystalline materials. Clarendon, Oxford
91. Sheng P (1980) Phys Rev B 21:2180
92. Paasch G, Smeisser D, Bartl A, Naarman H, Dunsch L, Göpel W (1994) Synth Met 66:135
93. Paul EW, Ricco AJ, Wrighton MS (1985) J Phys Chem 89:1441
94. Harsányi G (1995) Polymer films in sensor applications. Technomic, Basel, Switzerland
95. Pei Q, Inganäs O (1993) Synth Met 55–57:3730
96. Lepcsényi I, Reichardt A, Inzelt G, Harsányi G (1999) Highly sensitive and selective polymer based gas sensor. In: Proceedings of the 12th European Microelectronics and Packaging Conference, Harrogate, UK, 7–9 June 1999, pp 301–305
97. Inzelt G (2000) Electrochim Acta 45:3865
98. Monk PMS, Mortimer RJ, Rosseinsky DR (1995) Electrochromism. VCH, Weinheim, pp 124–143
99. Inzelt G, Csahók E, Kertész V (2001) Electrochim Acta 46:3955
100. Meerholz K, Heinze J (1996) Electrochim Acta 41:1839
101. Ping Z, Nauer GE, Neugebauer H, Thiener J, Neckel A (1997) J Chem Soc Faraday Trans 93:121
102. Diaz AF, Logan JA (1980) J Electroanal Chem 111:111
103. Genies EM, Penneau JF, Vieil E (1990) J Electroanal Chem 283:205
104. Horányi G, Inzelt G (1988) Electrochim Acta 33:947
105. Kalaji M, Peter LM (1991) J Chem Soc Faraday Trans 87:853
106. Feldberg SW (1984) J Am Chem Soc 106:4671
107. Rubinstein I, Sabatini E, Rishpon J (1987) J Electrochem Soc 134:3079
108. Diaz AF, Kanazawa KK, Gardini GP (1979) J Chem Soc Chem Commun, p 635
109. Kalaji M, Nyholm L, Peter LM (1991) J Electroanal Chem 313:271
110. Posadas D, Florit MI (2004) J Phys Chem B 108:15470
111. Otero TF, Grande HJ, Rodriguez J (1997) J Phys Chem B 101:3688
112. Feldberg SW, Rubinstein I (1988) J Electroanal Chem 240:1
113. Heinze J, Tschuncky P, Smie A (1998) J Solid State Electrochem 2:102
114. Vorotyntsev MA, Heinze J (2001) Electrochim Acta 46:3309

115. Pickup PG (1999) J Mater Chem 9:1641
116. Dennany L, Wallace GG, Forster RJ (2009) Langmuir 25:14053
117. Doblhofer K (1994) Thin polymer films on electrodes. In: Lipkowski J, Ross PN (eds) Electrochemistry of novel materials. VCH, New York, p 141
118. Doblhofer K (1992) J Electroanal Chem 331:1015
119. Doblhofer K, Vorotyntsev MA (1994) In: Lyons MEG (ed) Electroactive polymer electrochemistry, part 1. Plenum, New York, pp 375–437
120. Hillman AR, Loveday DC, Bruckenstein S (1989) J Electroanal Chem 274:157
121. Inzelt G, Bácskai J (1992) Electrochim Acta 37:647
122. Pruneanu S, Csahók E, Kertész V, Inzelt G (1998) Electrochim Acta 43:2305
123. Inzelt G, Horányi G (1987) J Electroanal Chem 230:257
124. Inzelt G, Kertész V, Nybäck AS (1999) J Solid State Electrochem 3:251
125. Buttry DA (1991) Applications of the quartz crystal microbalance to electrochemistry. In: Bard AJ (ed) Electroanalytical chemistry, vol 17. Dekker, New York, p 1
126. Inzelt G (1990) J Electroanal Chem 287:171
127. Inzelt G, Day RW, Kinstle JF, Chambers JQ (1983) J Phys Chem 87:4592
128. Inzelt G, Horányi G, Chambers JQ (1987) Electrochim Acta 32:757
129. Inzelt G, Chambers JQ, Kaufman FB (1983) J Electroanal Chem 159:443
130. Barbero C, Miras MC, Haas O, Kötz R (1991) J Electrochem Soc 138:669
131. Daifuku H, Kawagoe T, Yamamoto N, Ohsaka T, Oyama N (1989) J Electroanal Chem 274:313
132. Skompska M, Hillman AR (1997) J Electroanal Chem 433:127
133. Henderson MJ, Hillman AR, Vieil E (1999) J Phys Chem B 103:8899
134. Bácskai J, Martinusz K, Czirók E, Inzelt G, Kulesza PJ, Malik MA (1995) J Electroanal Chem 385:241
135. Karimi M, Chambers JQ (1987) J Electroanal Chem 217:313
136. Láng G, Bácskai J, Inzelt G (1993) Electrochim Acta 38:773
137. Oyama N, Oki N, Ohno H, Ohnuki Y, Matsuda H, Tsuchida E (1983) J Phys Chem 87:3642
138. Clarke AP, Vos JG, Hillman AR, Glidle A (1995) J Electroanal Chem 389:129
139. Chambers JQ, Kaufman FB, Nichols KH (1982) J Electroanal Chem 142:277
140. Baker CK, Qui YJ, Reynolds JR (1991) J Phys Chem 95:4446
141. Fiorito PA, Cordoba de Torresi SI (2005) J Electroanal Chem 581:31
142. Komura T, Mori Y, Yamaguchi T, Takahasi K (1997) Electrochim Acta 42:985
143. Ren X, Pickup PG (1992) J Electrochem Soc 139:2097
144. Orata D, Buttry DA (1987) J Am Chem Soc 109:3574
145. Barbero CA (2005) Phys Chem Chem Phys 7:1885
146. Barbero C, Miras MC, Kötz R, Haas O (1993) Solid State Ionics 60:167
147. Daikhin LI, Levi MD (1992) J Chem Soc Faraday Trans 88:1023
148. Amman E, Beuret C, Indermühle PF, Kötz R, de Rooij NF, Siegenthaler H (2001) Electrochim Acta 47:327
149. Troise Frank MH, Denuault G (1993) J Electroanal Chem 354:331
150. Bandey HL, Gonsalves M, Hillman AR, Glidle A, Bruckenstein S (1996) J Electroanal Chem 410:219
151. Barbero C, Calvo EJ, Etchenique R, Morales GM, Otero M (2000) Electrochim Acta 45:3895
152. Choi SJ, Park SM (2002) J Electrochem Soc 149:E26
153. Gabrielli C, Keddam M, Nadi N, Perrot H (2000) J Electroanal Chem 485:101
154. Varela H, Torresi RM (2000) J Electrochem Soc 147:665
155. Fehér K, Inzelt G (2002) Electrochim Acta 47:3551
156. Abrantes LM, Cordas CM, Vieil E (2002) Electrochim Acta 47:1481
157. Ansari Khalkhali R, Prize WE, Wallace GG (2003) React Funct Polym 56:141
158. Bruckenstein S, Brzezinska K, Hillman AR (2000) Phys Chem Chem Phys 2:1221
159. Gabrielli C, Garcia-Jareno JJ, Perrot H (2001) Electrochim Acta 46:4095
160. Weidlich CW, Mangold KM, Jüttner K (2005) Electrochim Acta 50:1547

161. Dang XD, Intelman CM, Rammelt U, Plieth W (2005) J Solid State Electrochem 9:706
162. Benito D, Gabrielli C, Garcia-Jareno JJ, Keddam M, Perrot H, Vicente F (2003) Electrochim Acta 48:4039
163. Chen SM, Fa YH (2004) J Electroanal Chem 567:9
164. Cintra EP, Torresi RM, Louarn G, Cordoba de Torresi SI (2004) Electrochim Acta 49:1409
165. White HS, Leddy J, Bard AJ (1982) J Am Chem Soc 104:4811
166. Vieil E, Meerholz K, Matencio T, Heinze J (1994) J Electroanal Chem 368:183
167. Abrantes LM, Correia JP, Savic M, Jin G (2001) Electrochim Acta 46:3181
168. Andrade EM, Molina FV, Posadas D, Florit MI (2005) J Electrochem Soc 152:E75
169. Bauerman LP, Bartlett PN (2005) Electrochim Acta 50:1537
170. Tallman DE, Pae Y, Bierwagen GP (1999) Corrosion 55:779
171. Lizarraga L, Andrade EM, Molina FV (2004) J Electroanal Chem 561:127
172. Nekrasov AA, Ivanov VF, Gribkova OL, Vannikov AV (2005) Electrochim Acta 50:1605
173. Nekrasov AA, Ivanov VF, Vannikov AV (2001) Electrochim Acta 46:3301
174. Otero TF, Rodríguez J (1994) Electrochim Acta 39:245
175. Puskás Z, Inzelt G (2005) Electrochim Acta 50:1481
176. Gabrielli C, Haas O, Takenouti H (1987) J Appl Electrochem 17:82
177. Armstrong RD (1986) J Electroanal Chem 198:177
178. Anson FC, Blauch DN, Saveant JM, Shu CF (1991) J Am Chem Soc 113:1922
179. Láng G, Inzelt G (1999) Electrochim Acta 44:2037
180. Láng GG, Ujvári M, Inzelt G (2004) J Electroanal Chem 572:283
181. Tu X, Xie Q, Xiang C, Zhang Y, Yao S (2005) J Phys Chem B 109:4053
182. Ujvári M, Láng G, Inzelt G (2000) Electrochem Commun 2:497
183. Gao Z, Bobacka J, Ivaska A (1994) J Electroanal Chem 364:127
184. Garcia-Belmonte G, Bisquert J (2002) Electrochim Acta 47:4263
185. Levi MD, Aurbach D (2002) J Electrochem Soc 149:E215
186. Vorotyntsev MA, Vieil E, Heinze J (1998) J Electroanal Chem 450:121
187. Komura T, Ishihara M, Yamaguti T, Takahashi K (2000) J Electroanal Chem 493:84
188. Levin O, Kontratiev V, Malev V (2005) Electrochim Acta 50:1573
189. Ivanova YN, Karyakin AA (2004) Electrochem Commun 6:120
190. Buck RP, Madaras MB, Mäckel R (1993) J Electroanal Chem 362:33
191. Buck RP, Mundt C (1999) Electrochim Acta 44:1999
192. Mathias MF, Haas O (1993) J Phys Chem 97:9217
193. Vorotyntsev MA, Badiali JP, Inzelt G (1999) J Electroanal Chem 472:7
194. Vorotyntsev MA, Daikhin LI, Levi MD (1994) J Electroanal Chem 364:37
195. Vorotyntsev MA, Deslouis C, Musiani MM, Tribollet B, Aoki K (1999) Electrochim Acta 44:2105
196. Zhang J, Zhao F, Abe T, Kaneko M (1999) Electrochim Acta 45:399
197. Tagliazucchi M, Calvo EJ (2010) ChemPhysChem 11:2957
198. Tagliazucchi M, Calvo EJ (2007) J Electroanal Chem 599:249
199. Marmisolle WA, Florit MI, Posadas D (2010) Phys Chem Chem Phys 12:7536
200. Bácskai J, Inzelt G (1991) J Electroanal Chem 310:379
201. Hillman AR, Bruckenstein S (1993) J Chem Soc Faraday Trans 89:339
202. Otero TF, Boyano I (2003) J Phys Chem B 107:6700
203. Lieder M, Schläpfer CW (1996) J Electroanal Chem 41:87
204. Mazeikiene R, Malinauskas A (1996) ACH Models Chem 133:471
205. Biaggio SR, Oliveira CLF, Aguirre MJ, Zagal JG (1994) J Appl Electrochem 24:1059
206. Brett CMA, Oliveira Brett AMCF, Pereira JLC, Rebelo C (1993) J Appl Electrochem 23:332
207. Rossberg K, Dunsch L (1999) Electrochim Acta 44:2061
208. Rourke F, Crayston JA (1993) J Chem Soc Faraday Trans 89:295
209. Yonezawa S, Kanamura K, Takehara Z (1995) J Chem Soc Faraday Trans 91:3469
210. Rossberg K, Paasch G, Dunsch L, Ludwig S (1998) J Electroanal Chem 443:49
211. Albery WJ, Elliot CM, Mount AR (1990) J Electroanal Chem 288:15

212. Ehrenbeck C, Jüttner K, Ludwig S, Paasch G (1998) Electrochim Acta 43:2781
213. Fletcher S (1993) J Chem Soc Faraday Trans 89:311
214. Bonazzola C, Calvo EJ (1998) J Electroanal Chem 449:111
215. Johnson BW, Read DC, Christensen P, Hamnett A, Armstrong RD (1994) J Electroanal Chem 364:103
216. Diaz AF, Bargon J (1986) In: Skotheim TA (ed) Handbook of conducting polymers, vol 1. Dekker, New York, pp 81–115
217. Tourillon G (1986) Skotheim TA (ed) Handbook of conducting polymers, vol 1. Dekker, New York, pp 293–350
218. Genies EM, Pernaut JM (1984) Synth Met 10:117
219. Tezuka Y, Aoki K, Shinozaki K (1989) J Electroanal Chem 30:369
220. Matencio T, Vieil E (1991) Synth Met 41–43:3001
221. de Gennes PG (1981) Macromolecules 14:1637
222. Peerce PJ, Bard AJ (1980) J Electroanal Chem 114:89
223. Bull RA, Fan JRF, Bard AJ (1982) J Electrochem Soc 129:1009
224. Carlin CM, Kepley LJ, Bard AJ (1986) J Electrochem Soc 132:353
225. Zotti G, Cattarin S, Comisso N (1988) J Electroanal Chem 239:387
226. Rydzewski R (1990) Continuum Mech Thermodyn 2:77
227. Inzelt G, Szabó L, Chambers JQ, Day RW (1988) J Electroanal Chem 242:265
228. Yang N, Zoski CG (2006) Langmuir 22:10328
229. Fraouna K, Delamar M, Andrieux CP (1996) J Electroanal Chem 418:109
230. Matencio T, Pernaut JM, Vieil E (2003) J Braz Chem Soc 14:1
231. Odin C, Nechtschein M (1991) Phys Rev Lett 67:1114
232. Odin C, Nechtschein M (1993) Synth Met 55–57:1281
233. Rodríguez Presa MJ, Posadas D, Florit MI (2000) J Electroanal Chem 482:117
234. Aoki K (1991) J Electroanal Chem 310:1
235. Aoki K (1994) J Electroanal Chem 373:67
236. Cao J, Aoki K (1996) Electrochim Acta 41:1787
237. Dietrich M, Heinze J (1991) Synth Met 41–43:503
238. Gottesfeld S, Redondo A, Rubinstein I, Feldberg SW (1989) J Electroanal Chem 265:15
239. Vorotyntsev MA, Badiali JP (1994) Electrochim Acta 39:289
240. Dunsch L, Rapta P, Neudeck A, Reiners RP, Reinecke D, Apfelstedt I (1996) Dechema Monographien 132:205
241. Aoki K, Edo T, Cao J (1998) Electrochim Acta 43:285
242. Grande H, Otero TF (1999) Electrochim Acta 44:1893
243. Otero TF, Grande H, Rodrigues J (1995) J Electroanal Chem 394:211
244. Aoki K, Cao J, Hoshino Y (1994) Electrochim Acta 39:2291
245. Aoki K, Kawase M (1994) J Electroanal Chem 377:125
246. Aoki K, Teragashi Y, Tokieda M (1999) J Electroanal Chem 460:254